The Kago low-sulfidation gold and silver deposit: A peripheral mineralization to the Nansatsu high-sulfidation system, Southern Kyushu, Japan

[1]Thomas TINDELL, [1]Koichiro WATANABE, [2]Akira IMAI, [2]Ryohei TAKAHASHI, [3]Adrian J. BOYCE, [1]Kotaro YONEZU, [4]Anders SCHERSTEN, [4]Laurence PAGE and [5]Takeyuki OGATA

[1]Department of Earth Resources Engineering, Kyushu University, Fukuoka, Japan

[2]Department of Earth Science and Technology, Akita University, Akita, Japan

[3]Scottish Universities Environmental Research Centre, Glasgow, UK

[4]Department of Earth and Ecosystem Science, Lund University, Sweden

[5]International Center for Research and Education on Mineral and Energy Resources, Akita University, Akita, Japan

Corresponding Author: tindell-tom@mine.kyushu-u.ac.jp

Abstract

The Kago deposit is a small deposit located at the southern tip of the Satsuma Peninsula of Southern Kyushu, Japan. It lies proximal to the well-known Nansatsu-type mineralization province dominated by high-sulfidation type epithermal deposits. The deposit was heavily mined in the 18th Century, largely for its relatively higher gold compared to that of surrounding and regional deposits. The Kago deposit is a typical low-sulfidation deposit, characterised by adularia-quartz veins, composed of electrum, Ag-tetrahedrite, polybasite, chalcopyrite and pyrite. Based on mine records, the grade ranged from 4.1-13.3 g/t Au and 2.6-6.6 g/t Ag. Alteration grades from low to high temperature argillic into a propylitic zone at the extremes of the vein exposures. Carbonate is absent. Fluid inclusion microthermometry reveals a typical temperature range of 220-240°C with salinity of 0.7-2.6 NaCl eq. wt%. Electrum from high-grade ore ranges from 66 to 69 wt% Au. $^{40}Ar/^{39}Ar$ age dating of adularia bearing colloform/crustiform and brecciated veins, suggests a mineralisation event from 4.23 to 4.0 Ma. $\delta^{18}O$ of veined and silicified quartz ranges from +4.0 to +18.4‰. $\delta^{18}O_{H_2O}$ of fluids in equilibrium with quartz, in the dominant range of measured fluid inclusion temperatures, ranges from -6.5‰ to -0.2‰. $\delta^{34}S$ of pyrite has a narrow range from -1.8 to 2.7 ‰. The deposit lies at the northern extent of the classic Nansatsu high-sulfidation epithermal area, in which a number of silicified bodies punctuate the region in a roughly semi-circular shape. The Kago deposit lies within the principle mineralisation age range of the high-sulfidation deposits, which range from 5.5 to 3.7 Ma. The structural displacement of the Kago deposit from the Nansatsu mineralisation and the differing host rocks has greatly influenced alteration, ore and rock-water interaction of the ore depositing fluids. Here we seek to establish the

relationship that this extended mineral province has between the differing styles of mineralisation.

Keywords: Kago, Nansatsu, gold, Ar/Ar, oxygen, sulfur

1. Introduction

Southern Kyushu is renowned for its abundance of epithermal mineralisation, in contrast to Northern Honshu, at the northern extreme of the main islands of Japan, which is dominated by Kuroko-type massive sulfide deposits of the "green tuff" regions (Lambert and Sato, 2008). The Southern province of Kyushu hosts a number of low- and high-sulfidation deposits along the Satsuma Peninsula (Figure 1a). The northern region of the peninsula is renowned for hosting the Kushikino and Hishikari low-sulfidation gold deposits (Takeuchi and Shikazono, 1984; Izawa et al., 1990). The Kago deposit is located in the Nansatsu district (Figure 1b), so called as it is in the Southern ("Nan") extreme of the Satsuma Peninsula. The Nansatsu district has three operating mines; Kasuga, Iwato and Akeshi. All mines are high-sulfidation-type and include native gold, enargite (except Akeshi, which hosts the enargite dimorph, luzonite), covellite, and pyrite. The descriptions of which were the subject of a seminal paper in the understanding of the development of epithermal systems (Hedenquist et al., 1994).. Commonly, gangue is dominated by quartz (>90%), goethite and scorodite. The silicified bodies are surrounded by a narrow advanced argillic zone, which grades out into argillic and regional propylitic zones. The Nansatsu ores are commonly regarded as relating to the eastward migration of the volcanic front, a consequence of the change in angle and rate of the descending slab of the Philippine sea-plate (Figure 2). All high-sulfidation deposits exhibit NE-SW orientated structural systems expressed as fracture (Iwato and Akeshi) or breccia systems (Kasuga).

The Kago low-sulfidation Au/Ag deposit is found in the north of the Nansatsu high-sulfidation Au system (Fig. 1a) and has been overlooked in geochemical terms, despite extensive local exploration. The Ministry of International Trade and Industry (MITI) published a report on deposits of the Nansatsu area, focusing on the Kago area mineralisations and outlying regional geology (MITI, 1998) (Fig. 1b). In this paper we examine the relationship between the Kago deposit and the existing high-sulfidation deposits to determine the genetic differences and similarities between the two contrasting epithermal systems. Here within, the depositional style is described in terms geochemistry, based on alteration mineralogy, vein textures and mineral geochemistry, microthermometry and stable isotope measurements. This is emphasised by the temporal relationship, revealed by $^{40}Ar/^{39}Ar$ age dating, which is compared to supporting ages from the Nansatsu District deposits. What becomes clear is the Kago deposit represents an episode of mineralization, peripheral to the principal Nansatsu high sulfidation deposits, exhibiting clear differences in fluid composition, which have greatly impacted on the behaviour and attributes of the deposited ores, alteration and gangue minerals.

2. Geological Setting

The basement of much of southern Kyushu Island and southwestern Shikoku Island comprises of the Shimanto-Supergroup, an accretionary prism of thickly bedded sandstones and interstratified

sandstone/mudstones. Tectonically these were likely deposited within an accretionary forearc basin, separated into Lower and Upper Units of Upper Cretaceous and Paleogene age (Taira et al., 1982). Repeated thrusting and erosion has exposed these units across southern Kyushu. Large-scale volcanism in southern Kyushu is related to the late Cenezoic subduction of the Philippine Sea plate, below the Eurasian plate, in which is sited most major epithermal mineralisations (Izawa and Urashima, 1989).

2.1 Local Stratigraphy

The Shimanto Supergroup terrane on Kyushu is separated into two units (Lower and Upper members), in which Southern Kyushu is covered by the Lower Shimanto Supergroup, locally composed of the Kawanabe Formation. Radiolarian age dating of the Lower Shimanto suggests an age of between 89.3 to 83.5 Ma (Terakoa and Kurimoto, 1986). Within the Nansatsu district, the Kawanabe Formation outcrops in the northwest and to a lesser extent in the southwest. Additionally, the Chiran Formation (Fig. 1b, in the NE), comprises sandstones and breccias which are extensively deposited several km to the central NW of the Satsuma Peninsula.

Volcanism of the magnetite series in the Satsuma region, is understood to have began in the late Miocene, later than 9 Ma (Izawa, 1992). In the central and southwest, the upper contact of the Kawanabe Formation forms an unconformity with the Nansatsu Group volcanic sequences and locally in the Kago area, tuffaceous brecciated sandstone/mudstones are recognised at the base of the Nansatsu Group (MITI, 1998) (Fig. 1b). The latter is separated into two formations, referred to as the Lower and Upper Formations. The Lower Formation is composed of pyroxene-hornblende andesite lavas, which have been dated by the whole rock K-Ar method, giving an age of 7.6 ± 2.3 Ma (MITI, 1985). The Upper Formation is composed of pyroxene andesite flows and related pyroclastics and volcaniclastics. The lower and upper horizons of the Upper Formation show K-Ar ages of 6.4 ± 0.3 Ma and 5.9 ± 0.8 Ma respectively (MITI, 1985). The northeast is composed of the Nansatsu Middle volcanics, composed of hornblende andesite and pyroclastic flows, of which the age range is about 4.6 to 2.7 Ma (MITI, 1992, 1996). Overlying the Cretaceous sediments and Upper Miocene to Lower Pliocene volcanic sequences are numerous Quaternary pyroclastic rocks. Ata Formation pyroclastics, erupted from Ata caldera towards the east of the Satsuma Peninsula, are distributed throughout the area. K-Ar age data gives a gross mean age of 108 ± 3 ka (Matsumoto and Ui, 1997). Later stage eruptions occurred from Aira caldera located in the centre of the Kagoshima graben (Fig. 2), which are sparsely observed in the north, central and east of the Nansatsu area. This is recognised as the Ito Formation and is dated by ^{14}C at 24.5 ka (Ikeda et al., 1995).

2.2 Structural Setting

Kyushu Island lies at the southwest extreme of the Median Tectonic Line (MTL), which runs roughly parallel to the fore-arc/back-arc division of the southern portion of Honshu (Fig. 2). The MTL extends to Kyushu where it crosscuts the island from NE to SW and is expressed as the Oita-Kumamoto Tectonic Line (OKTL). Along with the OKTL, the Northern and Southern Provinces are separated by the northeastern Hohi graben, the western Shimabara graben, and the Okinawa-trough, which extends

into the East China Sea (Kamata and Kodama, 1999). In the Southern Province, the Kagoshima graben dominates the region in a roughly NNE-SSW direction and hosts Quaternary to modern arc volcanism. Major caldera systems developed within the graben are similarly aligned forming the Kakuto, Aira and Ata calderas, delineating the present volcanic front. Much of the Satsuma peninsula experienced the effects of slab-roll back related calc-alkaline volcanism in the Miocene, caused by the older and more steeply dipping Philippine plate (Mahony et al., 2011). Locally, the Nansatsu District Quaternary volcanism covers much of the Nansatsu District, obscuring much of the earlier Cretaceous sediments and Miocene-Pliocene volcanic rocks. The mineralized high-sulfidation ore bodies conspicuously host northeast fracturing (Hedenquist et al., 1994), which is parallel to that of the Kago deposit veins.

2.3 Nansatsu District

The Nansatsu District is regarded as a type area of high-sulfidation deposits, dominated by intensely silicified bodies, produced by replacement of host lithology by low pH leaching and silica precipitation during the mixing of magmatic volatiles and local meteoric groundwaters (Hedenquist et al., 1994). These major deposits occur in a roughly semi-circular arcuate trend, with the exception of the youngest deposit, Akeshi, which is located just to the NE (Fig. 1a). The Shimanto Supergroup intersects this trend in the North, the cause of which is poorly understood. Structural faulting along the edge suggests formation of a caldera and the coastal outcrops of the Kurigano silicified body exhibit a sharp contact between Nansatsu Group andesites and the exposed Shimanto-Supergroup, hinting at a caldera system (Tindell et al., 2011). The eastward end of the Nansatsu region hosts the Ata caldera whose depression extends from land into the mouth of Kagoshima bay (Fig. 2). Distributed within the surficial caldera, clustered around Ikeda Lake, are a number of small-scale low-sulfidation type deposits, namely; Iiyama, Kuronida and Hanakago (Fig. 1a).

3. Mineralisation Ages

The age of mineralisation of the low and high-sulfidation epithermal deposits is extensively discussed in Watanabe (2005). Deposits situated in the Nansatsu district exhibit a younging direction from west to east. The Nansatsu high-sulfidation deposits situated on the western zone, are distributed around Makurazaki City. Mount Sonomi, about 2 km north of Kasuga mine, is a silicified body at the northern limits of the high-sulfidation zone, with a natroalunite K-Ar age of 5.5 ±0.4 Ma (Izawa, 1984). The Kasuga deposit has a K-Ar age in sericite (from alteration zone) of 4.3 ±0.2 Ma for the early stages of hydrothermal activity (Takeda et al., 2001). Alunite from the Iwato deposit shows a similar age range 4.4 ±0.7 Ma, whilst Akeshi deposit alunite shows 3.7 ± 1.1 Ma (Izawa, 1984). In the eastern zone of the Nansatsu region, the low-sulfidation deposits exhibit far younger ages. MITI (1985) dated adularia from the Iiyama deposit giving an age of 1.5 ± 0.1Ma, whilst Urashima and Ikeda (1987) dated adularia from Kuronida and Hanakago deposits (Fig. 1a), with ages of 1.3 ± 0.7 Ma and 1.1 ± 0.5 Ma respectively, suggesting a narrow range in which these deposits formed.

In the wider Satsuma area, the Hokusatsu district hosts two principle low-sulfidation deposits. The Kushikino deposit in the western region has an adularia K-Ar age of 3.35-3.69 Ma (MITI 2000, Izawa

and Zeng, 2001). The Hishikari deposit is situated to the east of the Kushikino deposit at the rim of the Kakuto caldera (the northern limit of the Kagoshima graben), and adularia age dating of successive veins in the group suggests an age range of 1.2-0.6 Ma (Sanematsu et al., 2005 and 2006).

4. Kago Au-Ag Deposit

The Kago Au and Ag mine operated from 1683 until the early 20th Century. The deposit, despite having a smaller excavatable area, was regarded as having a higher gold content to other deposits at the time, namely, Yamagano and Serigano deposits. Gold grades ranged from 4.1 to 13.3 g/t Au and 2.6 to 6.6 g/t Ag (Japan Mine Record, 1989).

The deposit is composed of a series of veins, which can be divided into 3 main groups; The Northern vein group (NVG), Central vein group (CVG) and the Southern vein group (SVG) (Fig. 1c). The NVG was not excavated to a great extent, hosting a small number of NE-SW striking veins, similar to the established trend of the CVG and NVG. However surficial exposure of veins is poor, due to heavy vegetation. MITI (1998) dated the K-Ar age of illite from a single vein, indicating an age of between 23.4 ± 0.7 to 22.8 ± 0.7 Ma. Based on the location of the vein and its corresponding age, it is likely related to the small ilmenite series granitic intrusions to the northeast (Ishihara and Matsuhisa 1999). The CVG and SVG compose the mining area, with which the SVG is a lower grade extension of the CVG. The CVG is where the majority of the mining operation took place and where surficial exposure of the main ore bearing veins remains. Major veins are aligned predominantly in a NE-SW direction (Fig. 1c). The SVG is an extension of the CVG major veins, but is largely barren and hosted in propylized rocks.

5. Analytical Procedure

5.1 Sampling Methodology

Samples were collected from surfical exposure of veins and wall rock and along tunnel roof and walls, in a roughly N-S direction across the CVG (Fig. 1c), based on the exposure of veins and surrounding altered wall rocks. In total 11 samples were collected for this study, with one additional sample of high-grade ore (YM-01) donated for electron probe microanalysis nd stable isotopic measurement. All collected samples were prepared for alteration, petrographic, $^{40}Ar/^{39}Ar$ age dating, fluid inclusion microthermometry and stable isotopic analysis.

5.2 Alteration mineralogy

Host rock samples immediately surrounding veined samples from the CVG were selected for analysis. Vein filling alteration minerals were not identified in the vein body, composed overwhelmingly of quartz and minor accessory adularia. Hydrothermal alteration minerals were determined by X-ray diffraction (XRD), following hydraulic elutriation treatment. Altered host rocks were lightly crushed in a stainless steel mortar. Samples were placed in distilled water and stirred in an ultrasonic bath. Samples were settled for 4 hours and the suspended < 2 μm fraction within 5 cm below the water

surface was siphoned and placed in a high-speed centrifuge at 4000 rpm for 20 minutes. Mineral separate was placed on thin sections and air-dried for XRD analysis. Orientated samples were analysed using a Rigaku Ultima IV X-ray diffractometer, operating at 40kV and 20mA with a CuKα ranging from 2.0-65.0 (2θ).

5.3 Vein and host rock petrography

Vein, breccia-veins and host rock samples were prepared as doubly polished thin-sections and polished sections.

5.4 Chemical composition of electrum

Electron probe micro analysis (EPMA) was carried out to determine the chemical composition of electrum from high-grade quartz vein breccia. Polished sections were measured using a JEOL JX-8800R. Analytical conditions were 20kV at a current of 20nA, using a prove diameter of 1μm. Au and Ag compositions were measured with LiF and PET-J crystals respectively. Standard materials used were JEOL pure metal standards Au and Ag.

5.5 $^{40}Ar/^{39}Ar$ age dating

The detection of adularia was identified by immersion of samples in dilute HF, followed by staining in sodium colbaltnitrite solution. The fine-grained samples from colloform/crustiform veins were separated by crushing and sieving in a 150-300μm fraction. Samples were treated by washing in a dilute acid (5% HF and 5% HNO_3) followed by cleaning in distilled water. Coarse-grained samples were separated from breccia veins and treated in dilute acid, followed by washing in distilled water. Finally crushed samples were analysed by XRD to ensure purity. Samples were irradiated with the Taylor Creek Rhyolite (TCR) sanidine standard (28.34 ±0.16 Ma; Renne et al., 1998) at the NRG-Petten HFR RODEO facility in the Netherlands. The mineral fractions were then step-heated using a defocused IR laser, they were then analysed using an electron multiplier on a Micromass-5400 Gas Source Mass Spectrometer, following the ^{40}Ar-^{39}Ar incremental heating method of Hermansson et al., (2008).

5.6 Fluid inclusion microthermometry

Fluid inclusions were measured using a Linkam cooling (L-600A) and heating (LK-600PM) systems and a Linkam FTIR-600 stage. Homogenisation temperature (T_h) was measured at a rate of 0.1°C/minute and the final ice melting temperature (T_m) was measured at a rate of 0.05°C/minute. Salinities were calculated based on the equations described in Bodnar, (1993).

5.7 Oxygen isotopic composition

For isotopic measurement, quartz was lightly crushed and treated in aqua-regia to remove any associated sulphides. Samples were then washed, air-dried and checked for impurities by X-ray

diffraction. Oxygen isotope analysis was by laser fluorination, involving total sample reaction with excess ClF_3 using a CO_2 laser as a heat source (in excess of 1500°C; following Sharp, 1990). All combustions resulted in 100% release of O_2 from the mineral lattice. This O_2 was converted to CO_2 by reaction with hot graphite, then analysed on-line by a VG Optima mass spectrometer. are reported in standard notation ($\delta^{18}O$) as per mil (‰) deviations from the Standard Mean Ocean Water (V-SMOW) standard. Standard materials analysed during the extraction of these samples were, SES, UWG2 and GP147 giving -10.1‰, 5.8‰ and 7.2‰ respectively, with a reproducibility of ± 0.2‰ (1σ).

5.8 Sulfur isotopic composition

The dominant sulfide in the majority of veins is pyrite. For representative veins, pyrite was separated and purified. Around 5 to 10mg was utilised for isotopic analysis. Minor contamination by non S-bearing phases was tolerated, and has no isotopic effect on the final data. Sulfides were analysed by standard techniques (Robinson and Kusakabe, 1975) in which SO_2 gas was liberated by combusting the sulfides with excess Cu_2O at 1075°C, *in vacuo*. Liberated gases were analysed on a VG Isotech SIRA II mass spectrometer, and standard corrections applied to raw $\delta^{66}SO_2$ values to produce true $\delta^{34}S$. The standards employed were the international standards NBS-123 and IAEA-S-3, and the SUERC standard CP-1. These gave $\delta^{34}S$ values of +17.1‰, -31.5‰ and -4.6‰ respectively, with 1σ reproducibility around ±0.2‰. Data are reported in $\delta^{34}S$ notation as per mil (‰) variations from the Vienna Cañon Diablo Troilite (V-CDT) standard.

6. Results

6.1 Alteration mineralogy

The host rock surrounding veins of the CVG is intensively altered at the immediate boundary of the veins. XRD measurement results for orientated samples are shown in Table 1; additional results are listed for samples collected from surficial outcrops and reported in MITI, 1997. Altered host rocks of adularia bearing veins are composed of illite and quartz. Additionally, host rocks of hydrothermal breccias, which bear adularia, contain illite. The thinner chalcedonic veins are enveloped by illite/smectite mixed layer minerals, with host rocks between veins (sample 100710-3) exhibiting illitic alteration. Silicification is present in brecciated veins, with mudstone clasts of the Kawanabe Formation partially replaced with quartz. These results suggest that the alteration is characteristically neutral to alkaline in nature. A composition of quartz, illite, illite/smectite indicates a high temperature argillic assemblage.

Results from the MITI 1997 report suggest a similar composition for veins within the CVG. The location of the measured alteration samples shows that they are situated in the SVG, which is largely hosted in the Nansatsu Upper Formation (Fig. 1c). The composition quartz, smectite ± plagioclase ± kaolinite was observed for all major and minor veining and may be attributed to both being peripheral to the CVG and the differing host rock. The existence of plagioclase maybe a product of regional propylization of the host rock, or a relic of the protolith.

6.2 Vein petrography and ore mineralogy

Veins may be categorized based on the texture and composition. All veins are dominated by quartz veining and here we will describe the various make up of vein groups.

6.2.1 CVG

Figure 3 shows a typical quartz vein ore sample from the CVG. Based on vein petrography, mineralization can be split into two major events. Initially, microcrystalline quartz and parallel bands of crustiform quartz are formed, with the early stage sporadically brecciated. A band of Ag-tetrahedrite, polybasite, and chalcopyrite with later covellite growth at the boundary between crustiform and microcrystalline quartz; electrum is sparsely distributed between these bands (Fig. 4, a & b).. Colloform banding is composed of quartz and successive fine-grained adularia, with later precipitated adularia of a fine to medium-grain size. This is followed by repeating bands of crustiform quartz, terminating at the contact with the Shimanto Supergroup host, which is composed of mixed clasts of microcrystalline quartz and Shimanto Supergroup mudstone, incorporation of both is likely related to the brecciated quartz vein that later follows (Fig. 3). Pyrite is disseminated at the early stage of crustiform growth, but is not recognised in the later crustiform or colloform bands. The later formed brecciated quartz vein is composed of crustiform, comb and microcrysatalline quartz, but is largely dismembered due to successive brecciation, obscuring the principle growth direction. Ore minerals are absent from this later stage that follows the banded earlier vein,

Hydrothermal breccias are a common feature of ores from the CVG, largely comprising cockade quartz/adularia, surrounding silicified clasts of the Shimanto Supergroup (Fig. 5a). Where host rock lithology is intact, it is composed of mudstone and sandstone interstratifications. Early precipitation on the clasts is of microcrystalline quartz, which is succeeded by lenticular parallel bands of adularia. Microcrystalline quartz makes up much of the matrix of the breccia. Pyrite is disseminated within the host rock clasts, but absent in the cockade quartz and adularia. Some brecciated rocks are largely composed of adularia infilling, clasts are composed of brecciated microcrystalline quartz veins and mudstone (Fig. 5b). Electrum-bearing banded veins, such as in Fig. 3 and Fig. 5c, show colloform adularia following the ore-bearing crustiform bands. Brecciation of the top contact wall rock is evident, but no mineralisation is associated with it.

High-grade ores of the CVG are composed of discontinuous quartz veins in brecciated and silicified mudstones of the Shimanto Supergroup. Colloform and crustiform bands are recognised in the earlier ore bearing veins, though these are not continuous, appearing brecciated. Large grains of electrum are recognised along the boundary of quartz and Shimanto Supergroup breccias and within ore bearing quartz veins. The electrum forms elongate agglomerations or anhedral grains of 0.05-2.0 mm in length (Fig. 6). The silicified rocks surrounding the high-grade ores are composed of brecciated clasts of Shimanto Supergroup and veined quartz. Pyrite is heavily disseminated and forms lenticular and euhedral crystals, which is largely composed of fine-grained quartz.

Several minor veins that crosscut the NE-SW trend of the major veins of the CVG (Fig. 1b) have textures that range from massive-quartz, microcrystalline-quartz and chalcedony-quartz. Electrum is rarely recognised within the disseminations, with a grain size of <0.05 mm, though pyrite is ubiquitous.

6.2.2 Quartz-Adularia Textures

Ore bearing bands as shown in figure 3 have barren parallel bands of quartz comprising microcrystalline quartz at the contact, which predominantly changes to a coarse mosaic texture and is overlain by a colloform band of quartz and crustiform adularia (Fig. 7a). The CVG hydrothermal breccias exhibit coarse-grained adularia, which has grown over mudstone clasts of the Shimanto Supergroup (Fig. 7b), followed by microcrystalline quartz. Pyrite is disseminated in the Shimanto Supergroup clasts with rare electrum. Fig. 7c shows an example of a chalcedony−quartz vein, which has largely recrystallized to quartz. In many cases the boundary of the vein is composed of a jigsaw pattern, which is followed by a layer of colloform bands, hosting a botryoidal textural pattern. Open spaces appear to have been filled by a chalcedonic precursor, which has recrystallized to flamboyant quartz (Fig. 7d and e). These are typically seen in the central area of veins, however at the termination of the vein a radial band is recognized before a final stage of jigsaw quartz. Moss texture is also recognised and is closely associated with colloform bands (Fig. 7f).

6.2.3 Electrum EPMA

Au and Ag ratio was measured from four electrum minerals from an ore sample of the CVG, totalling 24 analysis points. The weight percent (wt. %) Au and Ag is shown in Table 2. The composition of all analysed minerals is for the most part identical, with an Au maximum of 69.8 wt. % and a minimum of 66.1 wt. %. Ag shows a maximum of 33.0 wt. % and a minimum of 29.4 wt. %. No compositional zoning is identified from different measurement points from the same minerals.

6.3 ^{40}Ar/^{39}Ar age dating

Adularia was identified on three samples from the CVG. Colloform, crustiform and brecciated rocks. Fig. 5a-c, show the abundance of K-feldspar easily observed after sodium cobaltnitrite staining. The results of ^{40}Ar/^{39}Ar age measurement are shown in the age spectra of Fig. 8. The colloform banded adularia show an age of 4.23 ± 0.13 Ma. Hydrothermal breccia adularia was measured on two samples from two zones of adularia growth around separate cockade growth on host Shimanto Supergroup basement sediments: resulting in overlaping ages of 4.08 ± 0.04 Ma and 4.07 ± 0.03 Ma. Lastly, sample 090710-1 is composed of a thin vein (1cm width), which is largely composed of adularia in the matrix surrounding host rock clasts. Age was determined for two samples from the same breccia area. Results were 4.00 ± 0.03 Ma and 3.98 ±0.03 Ma.

Colloform quartz related adularia bands suggest an age of 4.23 ± 0.13 Ma. A larger than average error in this sample, maybe attributed to a higher quantity of quartz present in the sample. The colloform bands are followed by crustiform bands, which are in direct contact with brecciated wall rock (Fig. 5c). This is indicated primarily by the direction of growth of bands. Lack of a significant closing point on

the vein would suggest either that there has been significant movement from a parallel banded vein, resulting in this sample being a cohesive breccia clast, albeit a very large one (Fig. 3). Alternatively, the band is simply showing asymmetrical growth through periodic fracturing of the vein. This could be indicative of more unstable conditions continuing after principle vein mineralisation. Crustiform banding, which includes colloform quartz adularia bands, the maturation of these veins can be explained by episodic pressure release (Buchanan, 1981). Adularia-bearing brecciated veins, in which Shimanto Supergroup sediment are incorporated, may suggest a less complicated history of formation. Shimanto Supergroup mudstones are weakly silicified and contain pyrite disseminations. There are two bands of adularia precipitated around cockade clasts of Shimanto Supergroup mudstones. The initial band is very thin (0.5mm), which is followed by a layer of microcrystalline quartz and followed by the thicker second adularia band. The adularia precipitated here are the largest grains, being as big as 0.8cm in length (Fig. 5a). XRD analysis revealed a lack of significant quartz present in the band. The first and second bands give ages of 4.08 ± 0.04 and 4.07 ± 0.03 Ma respectively. In this case, the precision of the values indicates a negligible difference in the timing of mineralisation of successive bands. The brecciated quartz/adularia vein (fig. 5b) which is thinner than the former sample (1.5cm) shows similar mineralisation behaviour, in which early adularia is followed by precipitation of microcrystalline quartz. This is further brecciated with adularia in-filling. The ages produced from the earlier band (4.0 ± 0.03 Ma) and later infilling (3.98 ± 0.03 Ma) are indistinguishable.

6.4 Fluid inclusion microthermometry

Three separate vein classes were assessed for fluid inclusion microthermometry. CVG silicified breccia rocks, quartz vein and chalcedonic quartz veins. At least one sample from each representative class could be measured. Crustiform veins did not yield workable inclusions, being either sporadic or too small (<3μm).

In most cases inclusions are too small to be adequately measured (<3μm). However, some fluid inclusion assemblages could be defined by their morphology and inclusion characteristics: these are categorised into the following bi-phase and mono-phase types:

Type 1a - liquid-vapour: cubic- rectangular, lenticular, and in many cases, rounded or anhedral in form. Size ranges from 3-10μm and generally hosting a vapour phase of 15-30% total volume (Fig. 9). Primary in formation.

Type 1b – liquid-vapour: anhedral, with a characteristic "necking-down" form, largely indicative of reactivation of precipitation or healing of fracture induced nucleation. Vapour phase is uniform in liquid/vapour ratio. Likely secondary in nature.

Type 2 - Vapour-rich: Vapour hosting inclusions have very little or no visible liquid phase, these were not able to be analysed but represent a large proportion of inclusions. Unable to be assigned primary or secondary.

Type 3 - Liquid-only: Generally visible as planer secondary inclusions that have experienced necking down and usually accompanied by a small series of associated secondary liquid-vapour inclusions. A negative crystal form is common. Most likely secondary in nature.

Homogenisation temperature histograms are shown in Fig. 10 a, b and c and the associated salinities are listed in Table 3. Sample 300310-3 is composed of brecciated silicified rocks and finely brecciated vein quartz. High-grade ores are strongly correlated with silicification and brecciation like that demonstrated by this sample. Later stage quartz precipitation, typified by "vuggy" open space textures, contains inclusions following the path of growth zones or perpendicular to stages of growth. Homogenisation temperatures for Type 1a inclusions in 300310-3 range from 202°C to 221°C, with the mode in the 220°C field. T_m ranges from -0.4°C to -0.5°C, which corresponds to a salinity range of 0.7 to 0.9 NaCl equiv. wt%.

In sample 090710-5a, Type 3 single-phase liquid inclusions dominate. Areas of easily discernable growth contain numerous liquid inclusions, which are between 5-10μm in size. Type 1a liquid–vapour inclusions occur in swarms towards crystal terminations. Bi-phase inclusions are typically anhedral (Fig. 9), but lenticular forms are recognised perpendicular to growth zones. Variation of the liquid/vapour ratio is recognised in Type 1a inclusions. Abundant secondary inclusions are observed throughout the sample. Total homogenisation temperatures for Type 1a inclusions range from 169-270°C. When considering discrete FIAs, in which the necking-down phenomenon can be excluded, a strong modal composition is encountered at 220-230°C. Final ice melting temperatures (T_m) range from -0.3°C to -0.5°C, which corresponds to a calculated salinity of 0.5 to 1.0 NaCl equiv. wt%. The median salinity for the sample is 0.7 NaCl equiv. wt%.

Sample 090710-2, contain measureable inclusions in prismatic crystals, prior to precipitation of the flamboyant textured quartz. Type 1 inclusions are largely found in swarms at the central area of quartz crystals, these have an approximate size of 7μm, however, Type 3 mono-phase liquid inclusions dominate. Homogenisation temperatures for all Type 1a and 1b inclusions range from 220-287°C, with a strong mode at 230°C. T_m ranges from -1.0°C to -1.5°C which corresponds to salinites ranging from 1.7 to 2.7 NaCl equiv. wt%, with a median value of 2.0 NaCl equiv. wt%.

6.5 Oxygen isotopic composition

The $\delta^{18}O$ values for quartz are given in Table 4, and a histogram of measured $\delta^{18}O_{V\text{-}SMOW}$ for all quartz veins, silicified rocks chalcedonic and peripheral veins is shown in Fig. 11.. All recorded values are from the CVG and range from +4.0‰ to +13.1‰. Samples from the CVG surficial exposure have a relatively limited range (+7.3‰ to +9.1‰). Crustiform and brecciated rocks from the same vein (090710-5a and 090710-5b) vary slightly from +6.6‰ to +7.7‰. Colloform and brecciated samples that contain adularia (090710-1a and 090710-1b) are statistically indistinguishable (+5.8‰ to +5.9‰).

Silicified rock (300310-3) is similar to the range in exposed surficial CVG (+7.3‰). $\delta^{18}O$ of quartz from chalcodenic quartz veins show the highest $\delta^{18}O$ relative to other samples, 090710-2 having a value of +13.1‰. This is consistent with measurements of similar veins measured by MITI (1998; +11.4‰ to +18.4‰). $\delta^{18}O$ of quartz in exposed veins measured by MITI (1998) are slightly lower compared to that measured in this study (+4.0‰ to +5.9‰).

6.6 Sulfur isotopic composition

A small sample base of $\delta^{34}S$ was measured for pyrite hosted in veins or silicified rocks and is listed in Table 4. $\delta^{34}S$ ranges from -1.8‰ to +2.7‰. Pyrite derived from veined samples show lower $\delta^{34}S$ compared to those hosted in silicified breccia rocks.

7. Discussion

The geochemical and temporal relationship of the Kago deposit to its surroundings is of significance in understanding the evolution of the depositional behaviour of high-sulfidation and low-sulfidation deposits in Japan and related magmatic-hydrothermal arc systems. The proximity of the Kago and Nansatsu deposits offers us an opportunity, for the first time, to fully assess the temporal and geochemical differences on a local and regional scale.

7.1 Radiometric age and regional age associations

K-Ar radiometric age dating of the Kasuga, Iwato and Akeshi high-sulfidation deposits suggests that the principle mineralisation tootk place from 4.7 to 3.7 Ma (Fig 12). The larger silicified body Sonomi-dake, to the northeast of Kasuga, was also dated from alunite. This gave an age of 5.5 ± 0.4 Ma. Iwato deposit shows the largest spread of results, from its differing ore bodies; 4.7 ± 0.1 Ma, 4.4 ± 0.7 Ma and 4.15 ± 0.78 Ma. The larger errors from these results is likely due to the lower K concentration from alunites (Izawa, 1984).

The Kago deposit is situated approximately equidistant from Kasuga and Iwato (Fig. 1b) and the measured adularia of Kago, shows that mineralisation of took place between the onset of Iwato and the separate Akeshi mineralisation. Given the narrow spread in the $^{40}Ar/^{39}Ar$ data from Kago, it can be considered that 4.08 ± 0.03 Ma is statistically the most relevant, based on the very low error. When factoring in the surrounding deposits, which are locally emplaced in the caldera depression (Kasuga, Sonomi and Iwato), a sequence of activity may be seen. The earliest deposit to begin forming was the Sonomi silicified body, which was later followed by Kasuga. These deposits are aligned based on the dominant NE-SW regional structures. Whilst there is no age data for the Kurigano deposit, it is also emplaced along this trend. Following commencement of activity at Kasuga, the Kago deposit then began to form north-east of the Sonomi deposit, likewise following the NE-SW trend. In this case, we categorise the activity of Sonomi, Kasuga, Kago and possibly the Kurigano deposit within the same

structural framework. The Iwato deposit shares a similar age range as the Kasuga deposit and is likely formed by a parallel NE-SW trend on the eastern flank of the caldera.

The vein-type and silicified bodies of the Yamagawa area (Fig. 1a), in the south eastern Nansatsu area, host adularia mineralisation (Table 5). K-Ar ages support a later onset of mineralization, which is largely unrelated to the western Nansatsu and Kago deposits (Fig. 13) due to their very different age ranges (1.5 to 1.1 Ma) and Pleistocene-Pliocene Late Nansatsu volcanics hosts (Urashima and Ikeda, 1987). Table 5 shows the estimated age ranges for deposits in the Nansatsu and Hokusatsu regions and their associated alteration and mineralisation types.

7.2 Temperature and depth of formation

Fluid inclusion data in the Kago deposit suggest that there was a narrow range of mineralizing temperatures, between 220-240°C.. Lower temperature results observed in sample 090710-5a are recognised to be *type-1b* liquid/vapour inclusions and likely do not represent the true temperature of formation. Boiling is a common phenomenon that is related to ore mineralization in low-sulfidation epithermal deposits. In samples 090710-5a and 090710-2 a distinctive tail to higher temperature results is observed (Fig. 10) accompanied with the variation in vapor volume (15-30%), which may be related to the trapping of boiling vapour in an enclosing inclusion (Brown, 1998). If we consider that the ore fluids were boiling, we can estimate the palaeo-depth of the water table. Fig. 10, (*inset)* shows the boiling-point curves for fluids of 0.0 NaCl equiv. wt% and 2.0 NaCl equiv. wt% (Haas, 1971). Based on the principle modal homogenisation temperature and salinity from the representative samples, a depth of 256-305m below the palaeo-water table is estimated. With respect to the present structural configuration of the veins, 090710-5a is located +118 m above sea-level and 090710-2 is located +72 m above sea-level. Therefore giving a 46 m difference in their respective locations, this is very near the implied calculated depths. Additionally the higher temperature results of 090710-2 are located a deeper set of exposed veins.

7.3 Isotope geochemistry

$\delta^{18}O$ of quartz from crustiform, colloform vein quartz and silicified rocks vary from between +4.0‰ to +9.1‰. Fluid inclusion microthermometry homogenisation temperatures were used to assume the likely temperature of formation, for samples that did not contain measureable inclusions the modal temperature range of 220-240°C was applied. The $\delta^{18}O_{H_2O}$ in equilibrium with these measured values of quartz range from -4.7‰ to -0.3‰ using the fractionation equations of Clayton et al. (1972).

By contrast, chalcedonic veins characteristically have a higher $\delta^{18}O_{SMOW}$ value, ranging from 11.4‰ to 18.4‰. This is possibly caused by recrystallization of earlier formed silica (Dong et al., 1995) and is readily identified in the flamboyant texture in chalcedonic quartz veins (Fig. 7b-c). As such, the calculated $\delta^{18}O_{H_2O}$ for the range 220-240°C are around +1 to +9‰ and unlikely to be reliable. If the chalcedony were precipitated in equilibrium with the ore stage fluids, then the temperature of deposition would have been between 85 and 195°C (Table 4), assuming the composition range of fluids

calculated from quartz veins and silicified rocks (-4.7‰ to -0.3‰), using fractionation equations at low temperature (Kita et al., 1985).

The cause of $\delta^{18}O$ variation in the non-chalcodeny veins may result from a number of factors. Boiling of the hydrothermal fluids for the Kushikino low-sulfidation deposit in southern Kyushu area shows $\delta^{18}O_{SMOW}$ values range from +5.0‰ to +9.0‰ (Matsuhisa, 1986). However, Wagner et al (2005) modelled that boiling of mixed magmatic fluid drives precipitated quartz values to significantly higher $\delta^{18}O$ values, which does not account for the rather narrow and low $\delta^{18}O$ fluid values found in Kago. Thus, whilst evidence of boiling is observed in textures, it is unlikely to be the dominant mechanism for ore deposition.

Fluid mixing is another common phenomenon that is recognised in Kushikino and Hishikari as a possible mechanism for isotopic exchange (Faure et al, 2002). A value of -7‰ is assumed for typical meteoric waters in the Hokusatsu and Nansatsu areas (Matsuhisa and Aoki, 1994). Significant mixing of a deep hydrothermal fluid with ^{18}O-depleted meteoric waters will result in a decrease in the resultant $\delta^{18}O$ value. The $\delta^{18}O$ values of the Hishikari deposit show small variations with respect to early and later stage quartz/adularia banding. Matsuhisa and Aoki (1994) showed early stage quartz, associated with high grade 'ginguro' banding of sulfides and electrum from Hishikari, precipitated from a relatively ^{18}O-rich fluid, but the fluid became comparatively ^{18}O-depleted in later stages.

Rock-water interaction can strongly control the $\delta^{18}O$ of hydrothermal fluid. Shimanto Supergroup shales of the Hishikari deposit area are locally defined as the Morotsuka Group and correlate with the Kawanabe Formation (Izawa et al., 1990). Bulk rock $\delta^{18}O$ composition ranges from +10.5‰ to +14.4‰ (Takaoka, 1987). Naito (1993) showed the $\delta^{18}O$ of basement rocks of Hishikari were zoned, indicating a depletion in the $\delta^{18}O$ value in proximity to the vein wall.

$\delta^{34}S$ of pyrite range from -1.8‰ to +2.7‰. Basement rocks of the Shimanto Supergroup are known to be a poor source of S, with a range of -21.5‰ to -1.4‰ (Ishihara et al., 1986). A magmatic source is likely, given the homogeneity, and it is noteworthy that the $\delta^{34}S$ in Kago are similar to those found elsewhere in this belt (Hedenquist et al, 1994). Whilst the parent magnetite series granitoids from the Green Tuff region host an average $\delta^{34}S$ composition of +5.0‰ (Sasaki and Ishihara, 1979), Hedenquist et al (1994) note that a slight oxidation of the system (sulfide:sulphate = 3:1) could readily have produced the measured values. We cannot rule out a contribution of assimilation of Shimanto Supergroup to the magmatic system, albeit the homogeneity of Nansatsu S is notable (mean of Hedenquist and this study = -0.6 ± 2.8‰ (n =14)).

7.4 Geochemical associations

The ranges with which radiometrically determined ages conform to the locally hosted high-sulfidation deposits, suggest that Kago deposit is contemporaneous (Fig. 12). The residual silica, which forms the Kasuga high-sulfidation Au deposit, and the Iwato deposit, has a $\delta^{18}O$ composition of +9.3‰ to 11.1‰, which calculates to -2‰ to +2‰ for the ore forming fluids at 200-230°C (Hedenquist et al., 1994).

This would imply that the ^{18}O-depleted fluids of the Kago deposit show a slightly greater influence of meteoric fluids in the hydrothermal solutions. Sulfur is dominated by magmatic S in all deposits. The formation mechanisms of high-sulfidation deposits are substantially different to those of low-sulfidation deposits. Fracturing of host rocks promotes low-density vapour to pass into meteoric waters, thus acidifying them. The resultant low-pH fluid leaches the host rock and produces the characteristic advanced argillic alteration, characterised by silica and alunite (White, 1991). Conversely, in low-sulfidation deposition, where the boiling of fluids results in the loss of CO_2, the by-product is the precipitation of calcite and adularia (Hedenquist and Henley, 1985). Additionally, the route of fluids from their sources is substantially different. Rock-water reactions and inclusion of circulating meteoric waters that take place in low-sulfidation deposits (Simmons, 1995) suggests that depositing fluids are open to contact with surficial fluid. On the other hand, high-sulfidation deposits derive much of their metal transporting fluids from the magmatic volatiles or brines in deep-seated intrusives. These are essentially hypogene in their initial stages, rapidly transported through fractures and with minimal interaction with rock or meteoric fluids. Magmatic SO_2 disproportionates to form H_2S and H_2SO_4, which leach the host rock at the depositional zone and through interaction with meteoric fluids deposit their ore metals (e.g. Au and Cu). Alteration mineralogy in the depositional zones differs based on the vastly different pH conditions. Presence of illite, smectites surrounding veins and adularia in the veins of the Kago deposit, suggests a neutral pH condition. Whilst, the highly acidic nature of the early depositional vapour which leached out the original host rocks of the high-sulfidation deposits, indicates a low pH. This is witnessed by the presence of alunite and kaolinite of the advanced argillic zones. This gradually became more neutralised with increasing meteoric water influence over time.

Based on the structural associations between Kago and the principle Nansatsu deposits, the Kago deposit lies outside of the Shimanto Supergroup depression, but exhibiting the same NE-SW structural relationship. This indicates that since Nansatsu metal depositional fluids are intimately associated with magmatically-derived fluids, the Kago depositional zone is peripheral to this and derives a more significant element of its character from the surrounding meteoric fluids and host rocks, but acquiring its heat and perhaps metal transport complexes from the same deeply seated source.

7.5 Ore compositional variations in Nansatsu and Hokusatsu regions.

High-grade ores from the CVG show a propensity for >66 wt. % Au in electrum (Fig. 14). The Nansatsu high-sulfidation gold deposits are typically composed of native gold, although electrum is encountered at Iwato deposit. Urashima and Yamamoto (1981) observed compositional zoning within electrum, which has shown that the core of electrum at Iwato is Ag-rich, whilst the rim of electrum is Au-rich. Additionally, the presence of argentite, pyrargyrite and canfieldite at Iwato were encountered. Nonetheless, the electrum is much less silver rich than Kago (Fig. 14). Late-stage supergene oxidation is well recognised in high-sulfidation gold mineralization such as at Kasuga deposit, which shows remobilization of gold, associated with goethite and alteration minerals along fractures which host the highest grades (Hedenquist et al., 1994). Similarly, Iwato hosts higher grade Au from remobilization. The compositional zonation of Au and Ag in electrum in these deposits may be a function of the degree of oxidation. By comparison, the Kago deposit does not exhibit supergene or remobilization activity, so

these processes have not influenced the Au concentration of these ores. The Arakawa No. 4 vein of the Kushikino low-sulfidation deposit of the Hokusatsu region, which is larger in size and grade than Kago, hosts ore electrum compositions similar to that of Kago. Kushikino electrum ranges from the same, to slightly lower Ag content than that of Kago, ranging from 55 to 65 wt. % (Fig. 14). Takeuchi and Shikazono (1984) postulated that the presence of polybasite and sericite in the Arakawa No. 4 vein suggested a neutral to acidic pH condition. Variation of sericite and calcite precipitation is observed in the same mineralization episode at different elevations along the vein, with calcite poorly developed in the shallow levels, but conversely abundant in the deeper levels. There have been no reports of calcite present at Kago and it was not detected in this study, though we cannot rule out its existence in the deeper shoots of the veins. Furthermore, the Hishikari low-sulfidation deposit, largely known for it's bonanza level gold, ranges from 66-81% Au (Fig. 14). In the Honko deposit Au in electrum is elevated in higher levels of the veins, whilst electrum and sulfides decrease in abundance with depth (Izawa et al., 1990). Host rock interaction is particularly sensitive at Hishikari, in which much of the higher-grade zones are intimately associated with the unconformity between the Quarternary andesites and the underlying Shimanto Supergroup. Kago conversely, is situated wholly within the Shimanto Supergroup and does not show any unconformable or lithological boundary, this may have impacted on gold and silver precipitation, restricting the resultant grade.

8. Conclusions

The Kago deposit is peripheral to the denser population of high-sulfidation deposits that compose the southwestern Nansatsu District. Kago shows distinct characteristics, reflecting its low-sulfidation affiliation, and yet, our new dating indicates that the two deposit styles were contemporaneous around 4 Ma. What characterises Kago are:

1. A stronger meteoric influence in the mineralizing fluids, which nonetheless show significant water-rock interaction. The Nansatsu deposits, whilst having a significant meteoric influence show a lesser reaction of mineralizing fluids with the country rocks.

2. Fluid inclusion microthermometry suggests that the fluids precipitating quartz were boiling in the range 220-240°C. Salinities are typically from 0.7-2.7 NaCl equiv. wt%. $\delta^{18}O$ of quartz ranges from +4.0‰ to +9.1‰, which gives a $\delta^{18}O_{H_2O}$ of -6.5‰ to -0.3‰ for non-chalcedonic quartz. Mixing of fluids is strongly indicated by the $\delta^{18}O_{SMOW}$ composition. $\delta^{34}S$ compositions points to more magmatic influence on the S source, with little input from the Shimanto Supergroup.

3. The composition of electrum at Kago is comparable to other low-sulfidation deposits in the Hokusatsu District. Additionally, these are in stark contrast to that of the high-sulfidation

deposits, which are composed of native gold, a feature caused by oxidative supergene remobilisation.

4. NE-SW trending quartz-adularia veins, hydrothermal breccias and silicified Shimanto Supergroup mudstones. These are surrounded by high-temperature argillic and low-temperature argillic alteration in the CVG, suggesting a neutral pH condition. Conversely all high-sulfidation deposits show advanced argillic alteration, which is of a low pH.

Based on these characteristics, we define that the principle influence on mineralisation is the peripheral structural position of Kago, from the centre of hydrothermal activity defined by the high-sulfidation occurrences. Circulation of meteoric fluids plays an important role in the development of the veins, with periodic fracturing causing the strong brecciated manifestations and influencing Au-Ag precipitation.

Acknowledgements

We would like to express our sincere thanks to Eiji Izawa for his constant advise and expertise in this study. Additionally we are indebted to Masamichi Yamashita for donation of samples and Alison MacDonald at the Scottish Universities Environmental Research Centre for assistance with isotopic analysis. This study was supported by a Grant in-aid from the Global Center of Excellence in Novel Carbon Resource Science.

References

Bodnar, R. J. (1993) Revised equation table for determining the freezing point depression of H_2O-NaCl solutions. Geochim. Cosmochim. Acta, 57, 683-684.

Brown P. E. (1998) Fluid inclusion modelling for hydrothermal systems. In Richards, J. P. (ed.), Techniques in Hydrothermal Ore Deposits Geology, Reviews in Economic Geology, 10, 151-171.

Buchanan, L. J. (1981) Precious metal deposits associated with volcanic environments in the Southwest, Arizona Geological Society Digest, 14, 237-262.

Clayton, R.N., O'Neil, J.R. and Mayeda, T.K. (1972) Oxygen isotope exchange between quartz and water, J. Geophys. Res, 77, 3057-3067.

Dong, G., Morrison, G. and Jaireth, S. (1995) Quartz textures in epithermal veins, Queensland – Classification, origin and implication, Economic Geology, 90, 1841-1856.

Faure, K., Matsuhisa, Y, Metsugi, H., Mizota, C. and Hayashi, S. (2002) The Hishikari Au-Ag epithermal deposit, Japan: oxygen and hydrogen isotope evidence in determining the source of paleohydrothermal fluids. Economic Geology, **97**, 481-498.

Haas, J. L. (1971) Effects of salinity on maximum thermal gradient of a hydrothermal system at hydrostatic pressure, Economic Geology, 66, 940-946.

Hayashi, T. (2001) Geology and gold exploration in the Nansatsu District, southern Kyushu, Japan, Society of Economic Geologists Guidebook Series, 34, 127-132.

Hedenquist, J. W. and Henley, R. W. (1985) The importance on freezing point measurements of fluid inclusions: Evidence from active geothermal systems and implications for epithermal ore deposition, Economic Geology, 80, 1379-1406.

Hedenquist, J. W., Matsuhisa, Y., Izawa, E., White, N. C., Giggenbach, W. F. and Aoki, M. (1994) Geology, geochemistry, and origin of high-sulfidation Cu-Au mineralization in the Nansatsu District, Japan, Economic Geology, 89, 1-30.

Hermansson, T., Stephens, M. B. and Page, L. M. (2008) 40Ar/39Ar hornblende geochronology from the Forsmark area in central Sweden: Constraints on late Svecofennian cooling, ductile deformation and exhumation, Precambrian Research, 167, 303-315.

Ikeda, A., Okuno, M., Nakamura, T., Tsutsui, M. and Kobayashi, Y. (1995) Accelerator mass spectrometric 14C dating of charred wood in the Osumi pumice fall and Ito ignimbrite from Aira caldera, southern Kyushu, Japan, Quaternary Research, 34, 377-379.

Ishihara, S. and Matsuhia, Y. (1999) Oxygen isotopic constraints on the geneses of the Miocene Outer Zone granitoids in Japan, Lithos, 46, 523-534.

Ishihara, S., Sakamaki, Y., Sasaki, A., Teraoka, Y. and Terashima, S. (1986) Role of the basement in the genesis of the Hishikari gold-quartz vein deposit, southern Kysuhu, Japan, Mining Geology, 36, 495-509.

Izawa, E. (1992) Evolution of volcanic and hydrothermal systems in southern Kyushu, Geological Survey of Japan, Report No. 279, 84-88.

Izawa, E. and Urashima, Y. (1989) Quaternary gold mineralization and its geological environments in Kyushu, Japan, Economic Geology Monograph, 6, 233-241.

Izawa, E., Urashima, Y. and Okubo, Y. (1984) Age of mineralization of the Nansatsu type gold deposits, Kagoshima, Japan – K-Ar dating of alunites from Kasuga, Iwato and Akeshi, Mining Geology, 34, 343-351. (In Japanese, with English Abstract).

Izawa, E., Urashima, Y., Ibaraki, K., Suzuki, R., Yokoyama, T., Kawasaki, K., Koga, A. and Taguchi, S. (1990) The Hishikari gold deposit: high-grade epithermal veins in Quaternary volcanics of southern Kyushu, Japan, Journal of Geochemical Exploration, 36, 1-56.

Izawa E. and Zeng N. (2001) Kushikino gold mineralization in a Pliocene volcanic region, Kyushu, Japan, Economic Geology Guidebook Series, 34, 53-60.

Japan Mine Record (1989) The Mining and Materials Processing Institute of Japan, vol. 1, 111-114.

Kamata, H. and Kodama, K. (1999) Volcanic history and tectonics of the southwest Japan arc, Island Arc, 8, 393-403.

Kita, I., Taguchi, S. and Matsubaya, O. (1985) Oxygen isotope fractionation between amorphous silica and water at 34-93°C, Nature, 314, 83-84.

Lambert, I. B. and Sato, T. (2008) The Kuroko and associated ore deposits of Japan; A review of their features and metallogenesis, Economic Geology, 69, 1215-1236.

Mahony, S. H., Wallace L., Miyoshi, M., Villamor, P., Sparks, R., Hasenaka, T. (2011) Volcano-tectonic interactions during rapid plate-boundary evolution in the Kyushu region, SW Japan, Geological Society of America Bulletin, 123, 11-12, 2201-2223.

Matsuhisa, Y. (1986) Effect of mixing and boiling of fluids on isotopic compositions of quartz and calcite from epithermal deposits, Mining Geology, 36, 487-493.

Matsuhisa, Y., and Aoki, M. (1994) Temperature and oxygen isotope variations during formation of the Hishikari Epithermal gold-silver veins, southern Kyushu, Japan. Economic Geology, **89**, 1608–1613.

Matsumoto, A. and Ui, T. (1997) K-Ar age of Ata pyroclastic flow deposit, southern Kyushu, Japan, Bull. Volcanological Soc. Japan, 42, 223-225 (In Japanese).

Ministry of International Trade and Industry (MITI) (2000) Report of the 1999 Fiscal Year Geological Survey: Nansatsu Area. (In Japanese).

MITI (2000) Report on the 1999 Fiscal Year Geological Survey: Hokusatsu-Kushikino Area. (in Japanese).

MITI (1998) Report of the 1997 Fiscal Year Geological Survey: Nansatsu Area. (In Japanese).

MITI (1997) Report of the 1996 Fiscal Year Geological Survey: Nansatsu Area. (In Japanese).

MITI (1996) Report of the 1995 Fiscal Year Geological Survey: Nansatsu Area. (In Japanese).

MITI (1992) Report of the 1991 Fiscal Year Geological Survey: Nansatsu Area. (In Japanese).

MITI (1985) Report of the 1984 Fiscal Year Geological Survey: Nansatsu Area. (In Japanese).

Naito, K (1993) Occurrences of quartz veins in the Hishikari gold deposit, southern Kyushu, Japan, Resource Geology, Special Issue, 14, 37-45.

Renne, P. R., Swisher, C. C., Deino, A. L., Karner, D. B., Owena, T. L., DePaolo, D. J. (1998) Intercalibration of standards, absolute ages and uncertainties in $^{40}Ar/^{39}Ar$ dating. Chemical Geology, 145, 117-152.

Robinson, B.W., and Kusakabe, M., 1975, Quantitative preparation of SO_2 for $^{34}S/^{32}S$ analysis from sulfides by combustion with cuprous oxide: Analytical Chemistry, **47**, 1179-1181.

Sanematsu, K., Duncan, R., Imai, A. and Watanabe, K. (2005) Geochronological constraints using 40Ar/39Ar dating on the mineralization of the Hishikari epithermal gold deposit, Japan, Resource Geology, 55(3), 249-266.

Sanematsu, K., Watanabe, K., Duncan, R.A., Izawa, E. (2006) The history of vein formation determined by $^{40}Ar/^{39}Ar$ dating of adularia in the Hosen-1 vein at the Hishikari epithermal gold deposit, Japan, Economic Geology, **101**, 685-698.

Sasaki, A. and Ishihara, S. (1979) Sulfur isotopic composition of the magnetite-series and ilmenite-series granitoids in Japan, Contributions to Mineralogy and Petrology, 68, 107-115.

Sharp, Z.D., 1990, A laser-based microanalytical method for the in situ determination of oxygen isotope ratios in silicates and oxides: Geochimica Cosmochimica Acta, v. 54, 1353-1357.

Simmons, S. F. (1995) Magmatic contributions to low sulfidation epithermal deposits, in Thompson, J. F. H., ed., Magmas, fluids and ore deposits: Mineralogical Association of Canada Short Course Handbook, V. 23, 455-478.

Taira, A., Okada, H., Whitaker J. H. and Smith, A. J. (1982) The Shimanto Belt of Japan: Cretaceous-lower Miocene active-margin sedimentation, Geological Society of London, Special Publication, 10.1, 5-26.

Takaoka, H. (1987) Final report on the case study of oxygen isotopic exploration (Hishikari and Urushi-Ora areas), Tech, Rep. Mines Resour. Div. Sumitomo Metal Mining, 4: 1-.17 (in Japanese).

Takeda, T., Shimada, N., Ueno, H. (2001) Paleomagnetic constraints on mineralization age of the Nansatsu-type gold deposits in southern Kyushu, Japan, Resource Geology, 51, 239-248.

Takeuchi, K. and Shikazono, N. (1984) Mineralization of the Arakawa No. 4 vein of the Kushikino mine, Kagoshima Prefecture, Japan, Mining Geology, 34, 187-195.

Teraoka, Y. and Kurimoto, C. (1986) Cretaceous stratigraphy of the Shimanto Terrane in the Uwajima area, west Shikoku, southwest Japan, with reference to the stratigraphic distribution of mega- and radiolarian fossils, Bull. Geol. Surv. Japan, 37, 417-453 (in Japanese).

Tindell, T., Watanabe, K., Imai, A., Takahashi, R. and Boyce, A. J. (2011) Mineralisation and alteration characteristics of the Kasuga area peripheral silicified bodies, Nansatsu District, Japan, In proceedings of the 1st Asia Africa Mineral Resources Conference.

Urashima, Y., Ueno, T., Miyauchi, N. and Yamashita, S. (1990) Coarse-grained gold (Toji-kin) bearing ores from the Yamagano, Akeshi, Kasuga, and Kago mines, Kagoshima Prefecture, Japan, in

Organization of Prof. Y. Urashima retirement ceremony (ed.) Professor Yukitoshi Urashima Commemoration Volume on the Occasion of his Retirement, 1-15 (in Japanese).

Urashima, Y., Ikeda, T., (1987) K-Ar ages for adularia from the Fuke, Okuchi, Hishikari, Kuronita, and Hanakago gold-silver deposits, Kagoshima Prefecture, Japan, Mining Geology, 37, 205-213. (In Japanese, with English Abstract).

Urashima, Y. and Yamamoto, S. (1981) The Iwato gold ore deposits, Kagoshima Prefecture, Japan, Mining Geology Special Issue, 10, 1-14 (in Japanese with English abstract).

Wagner, T., Williams-Jones, A.E. and Boyce, A.J. (2005) Stable isotope-based modelling of the origin and genesis of an unusual Au-Ag-Sn-W epithermal system at Cirotan, Indonesia. Chemical Geology, **219**, 237-260.

Watanabe, Y. (2005) Late Cenozoic evolution of epithermal gold metallogenic provinces in Kyushu, Japan, Mineralium Deposita, 40, 307-323.

White, N. C. (1991) High sulfidation epithermal gold deposits: Characteristics and a model for their origin: Geological Survey of Japan, Report No. 277, 9-20.

Figures

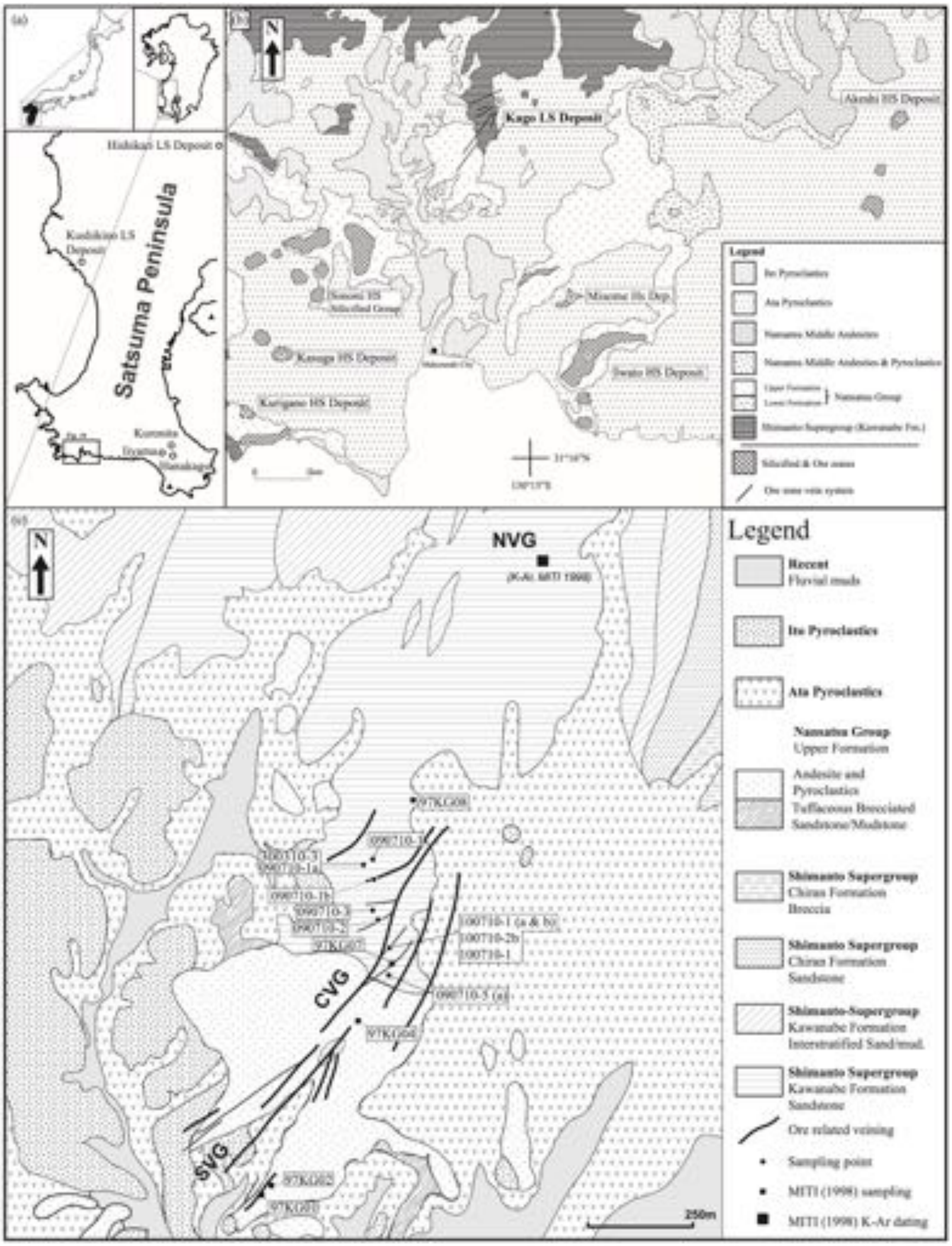

Fig. 1

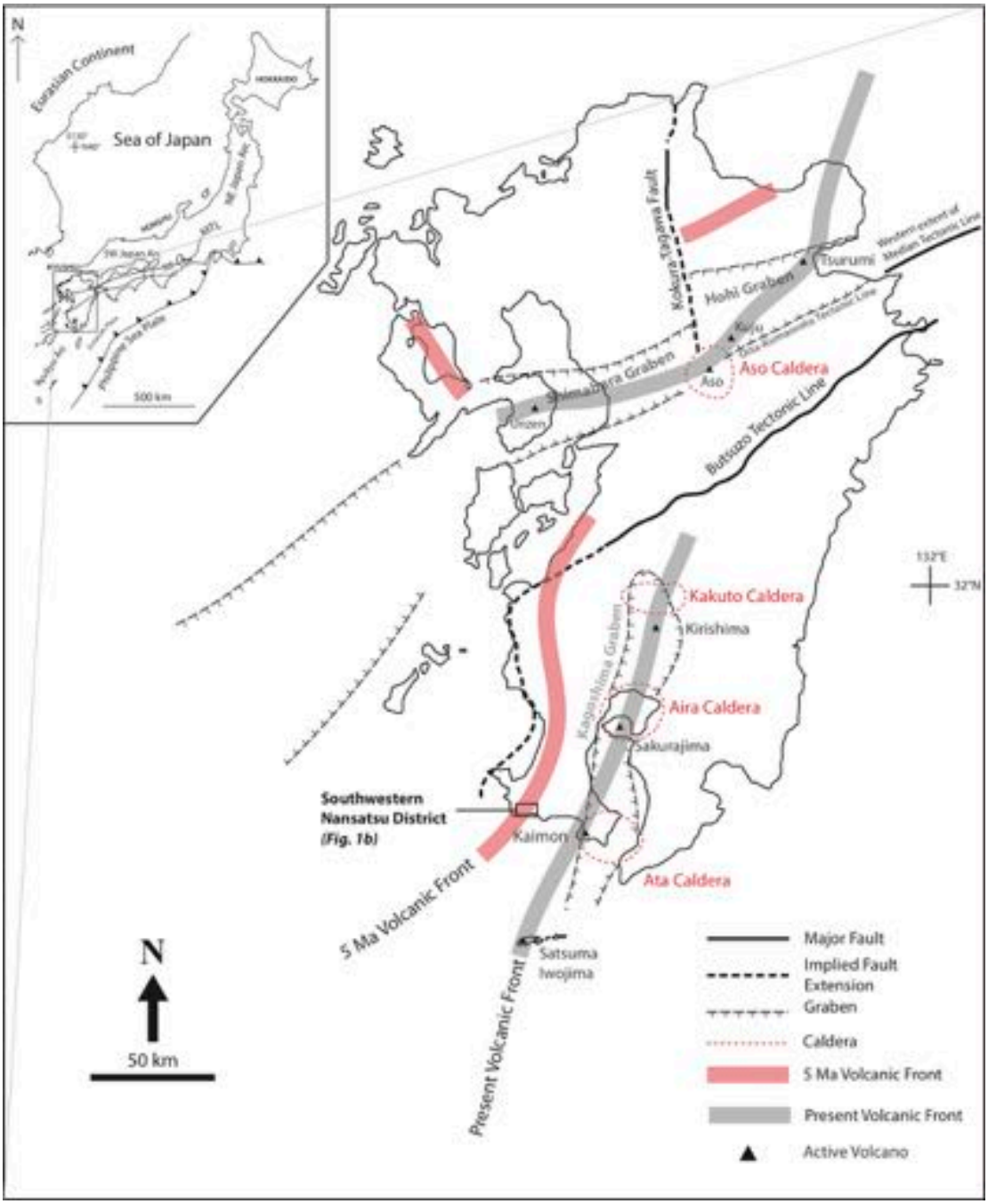
N
Eurasian Continent
Sea of Japan
HOKKAIDO
500 km
Philippine Sea Plate
Kokura-Tagawa Fault
Hohi Graben
Tsurumi
Western extent of Median Tectonic Line
Kuju
Oita-Kumamoto Tectonic Line
Aso Caldera
Aso
Unzen
Shimabara Graben
Butsuzo Tectonic Line
132°E
32°N
Kakuto Caldera
Kirishima
Kagoshima Graben
Aira Caldera
Sakurajima
Southwestern
Nansatsu District
(Fig. 1b)
Kaimon
Ata Caldera
5 Ma Volcanic Front
Satsuma
Iwojima
Present Volcanic Front
N
50 km
Major Fault
Implied Fault
Extension
Graben
Caldera
5 Ma Volcanic Front
Present Volcanic Front
Active Volcano

Fig. 2

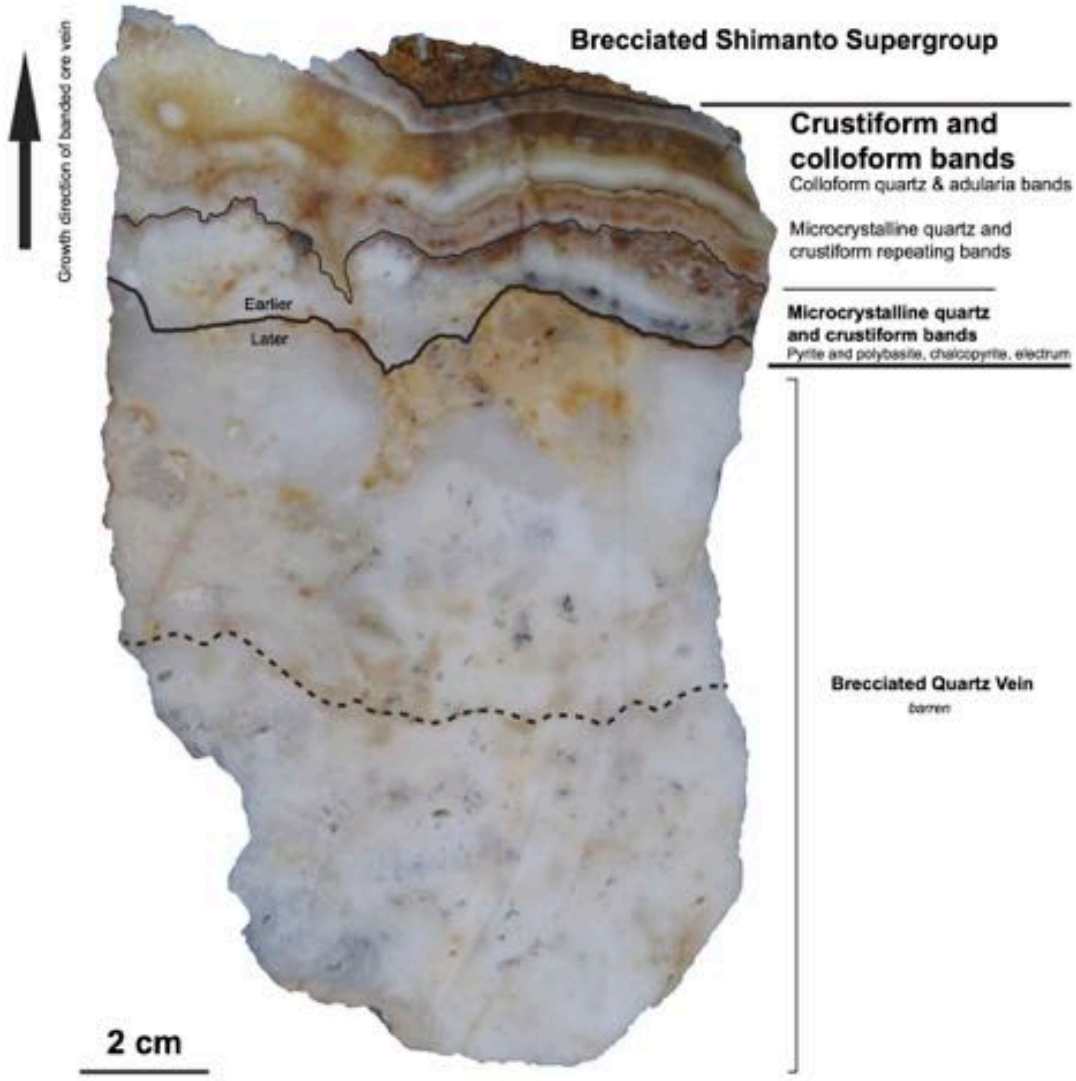
Growth direction of banded ore vein
Brecciated Shimanto Supergroup
Crustiform and colloform bands
Colloform quartz & adularia bands
Microcrystalline quartz and crustiform repeating bands
Earlier
Later
Microcrystalline quartz and crustiform bands
Pyrite and polybasite, chalcopyrite, electrum
Brecciated Quartz Vein
barren
2 cm

Fig. 3

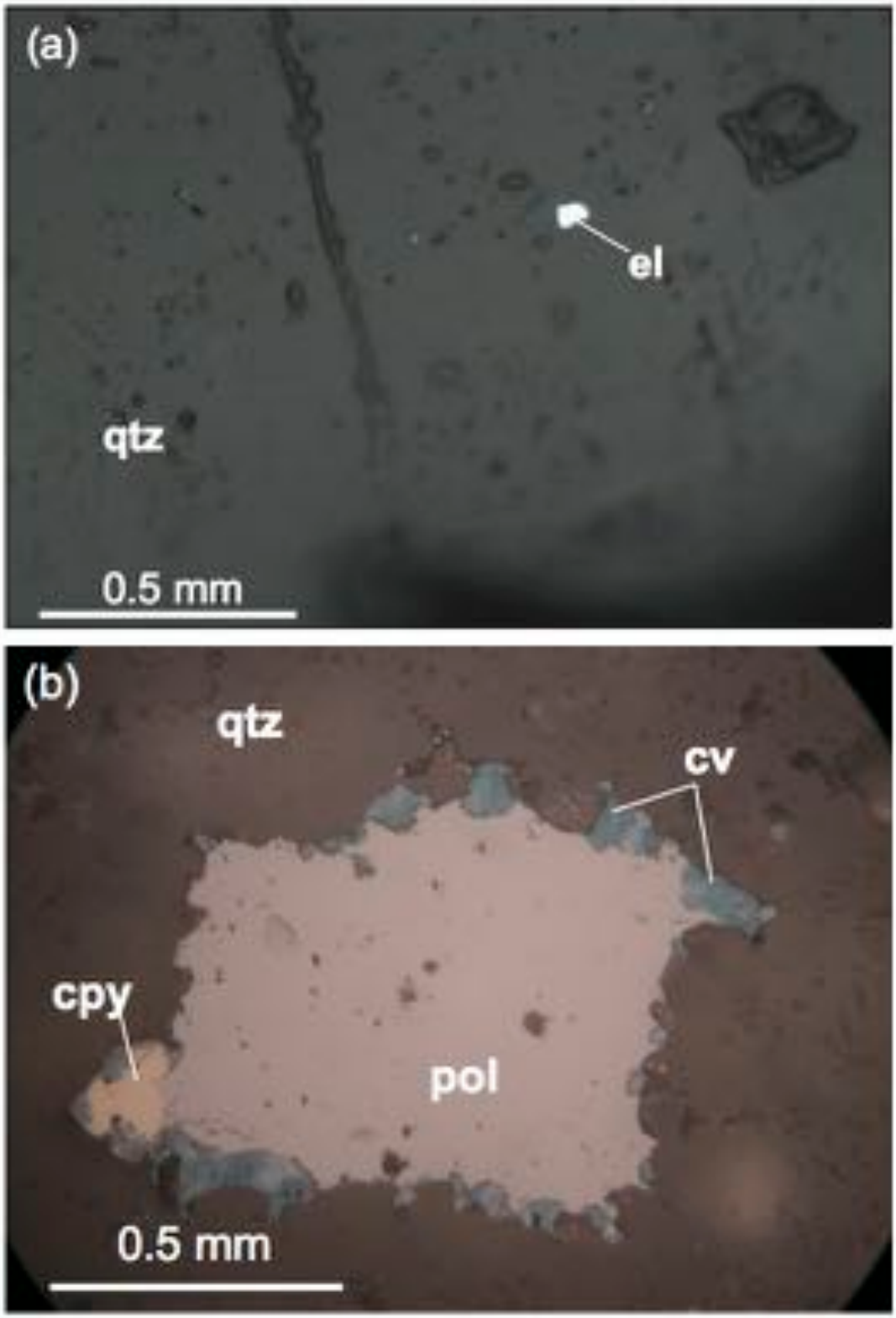

Fig. 4

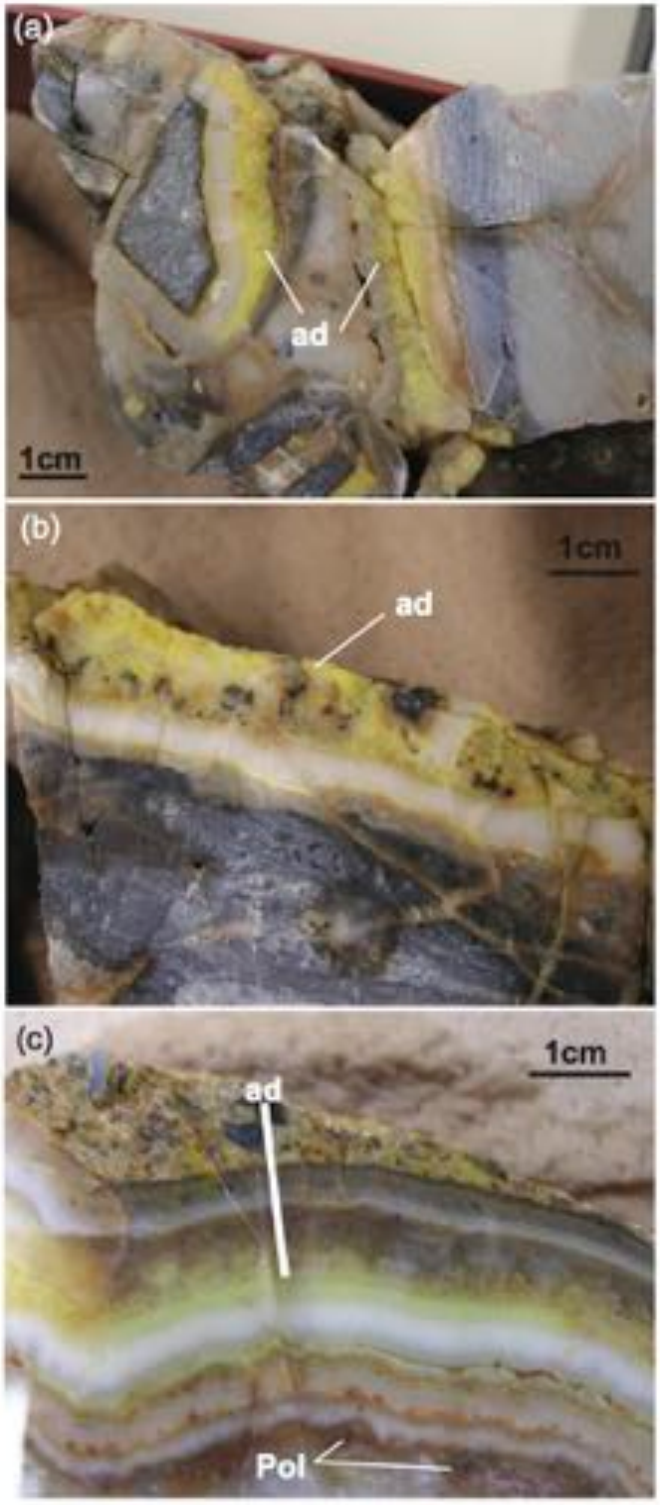

Fig. 5

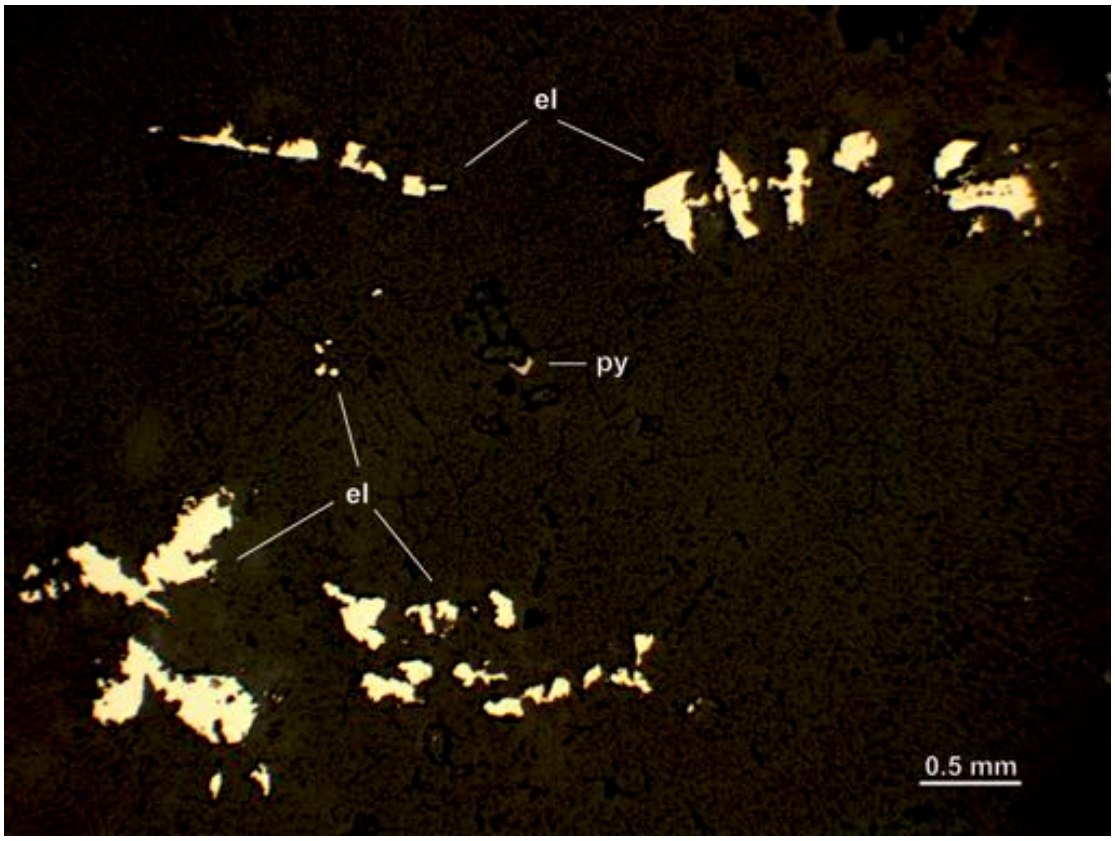

Fig. 6

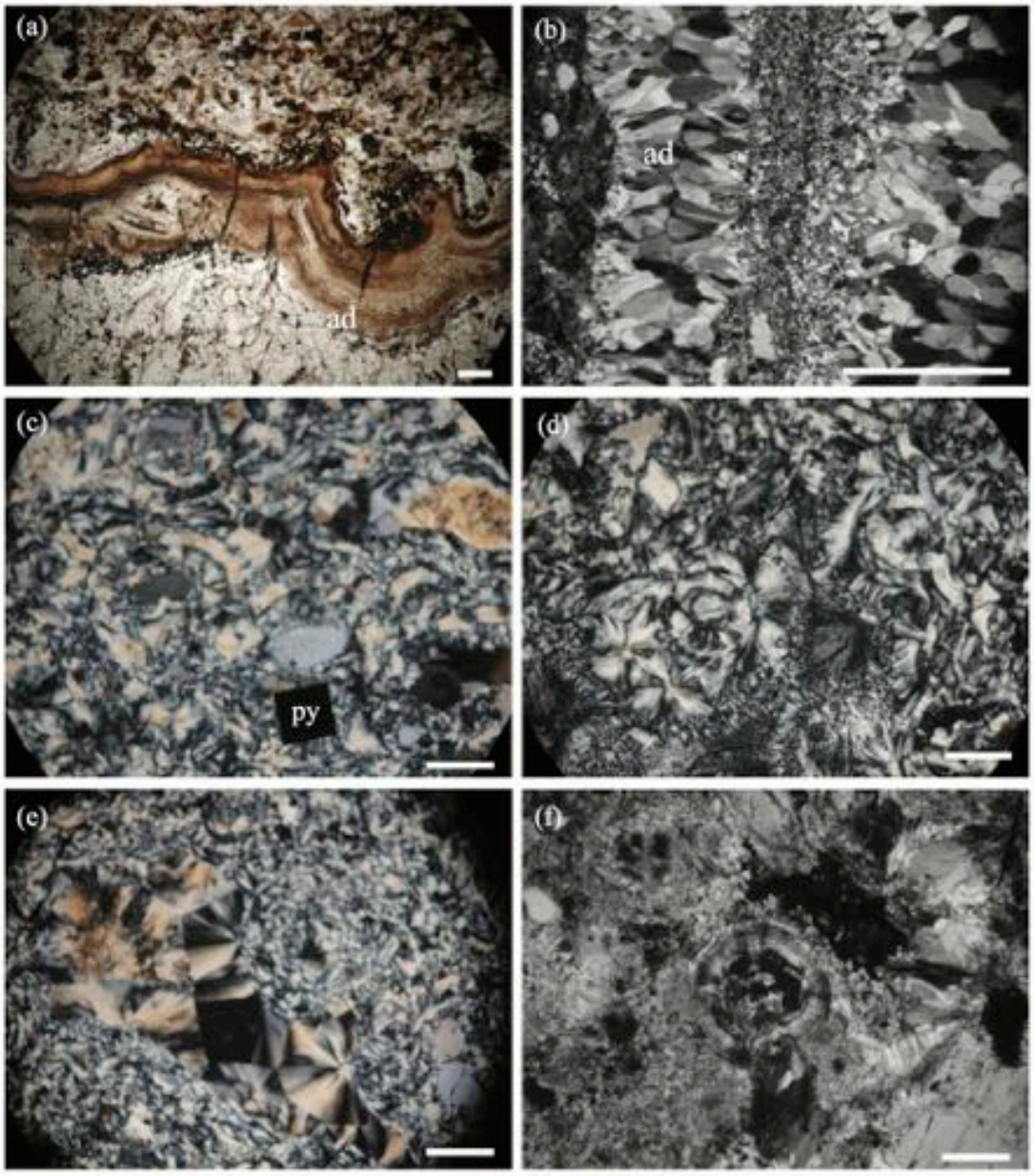

Fig. 7

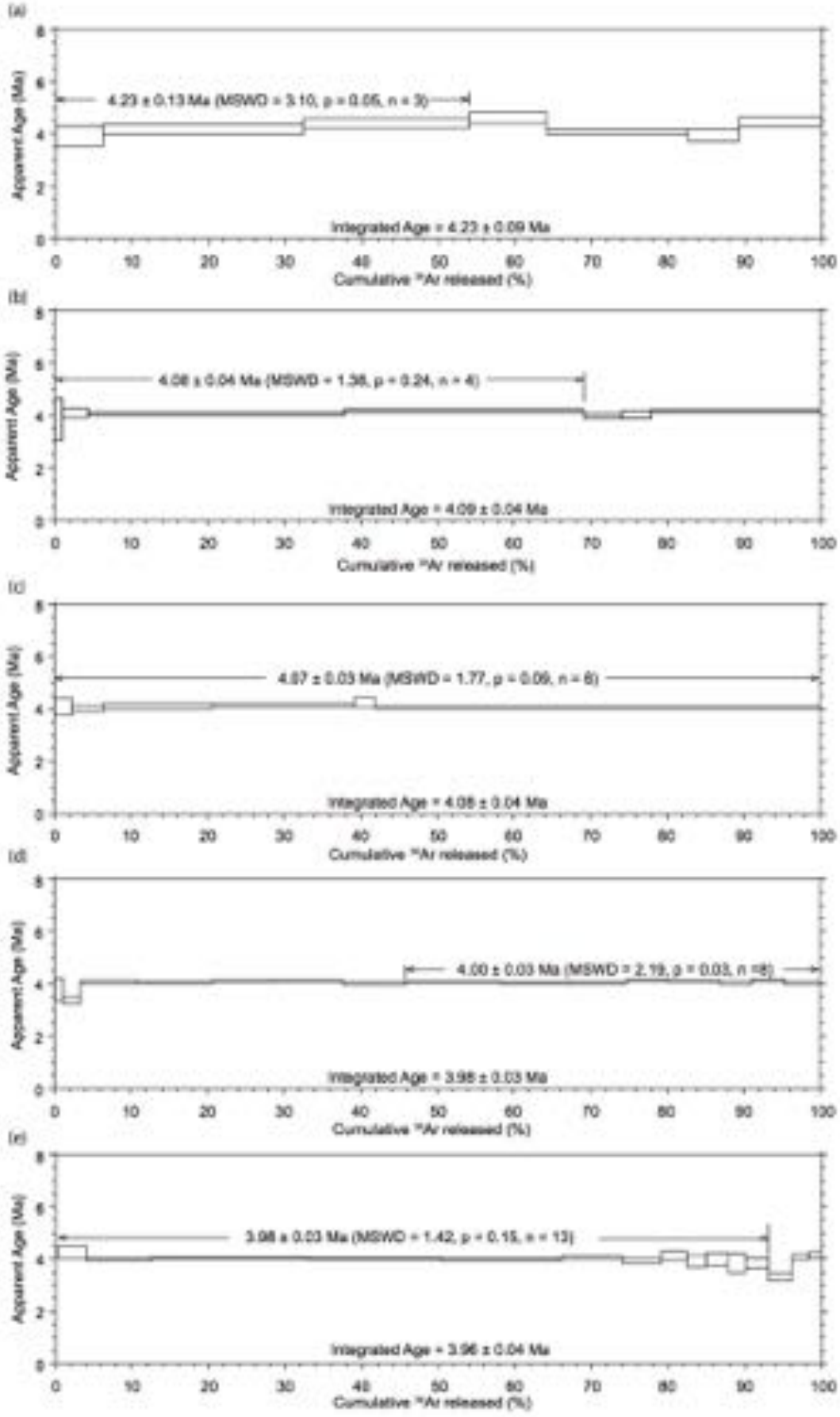
(a)
4.23 ± 0.13 Ma (MSWD = 3.10, p = 0.05, n = 3)
Integrated Age = 4.23 ± 0.09 Ma
Apparent Age (Ma)
Cumulative ³⁹Ar released (%)
(b)
4.08 ± 0.04 Ma (MSWD = 1.38, p = 0.24, n = 4)
Integrated Age = 4.09 ± 0.04 Ma
Apparent Age (Ma)
Cumulative ³⁹Ar released (%)
(c)
4.07 ± 0.03 Ma (MSWD = 1.77, p = 0.09, n = 6)
Integrated Age = 4.08 ± 0.04 Ma
Apparent Age (Ma)
Cumulative ³⁹Ar released (%)
(d)
4.00 ± 0.03 Ma (MSWD = 2.19, p = 0.03, n =8)
Integrated Age = 3.98 ± 0.03 Ma
Apparent Age (Ma)
Cumulative ³⁹Ar released (%)
(e)
3.98 ± 0.03 Ma (MSWD = 1.42, p = 0.15, n = 13)
Integrated Age = 3.96 ± 0.04 Ma
Apparent Age (Ma)
Cumulative ³⁹Ar released (%)

Fig. 8

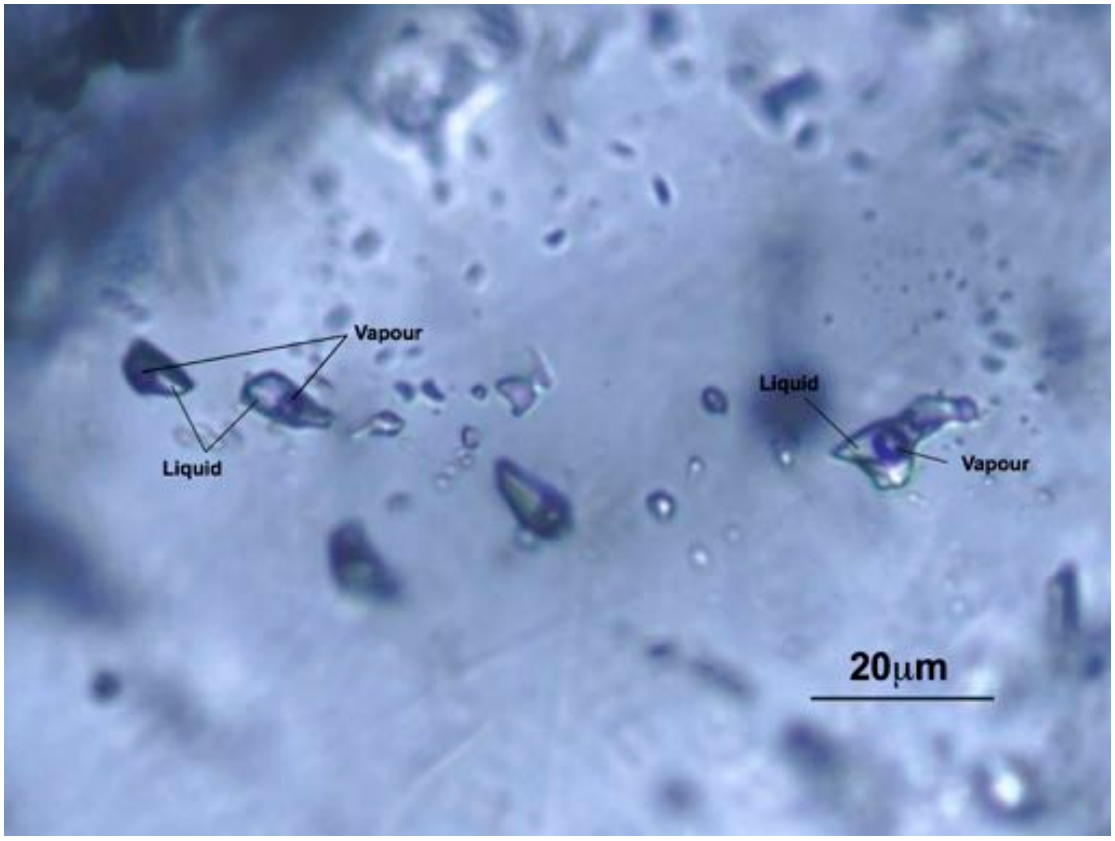

Fig. 9

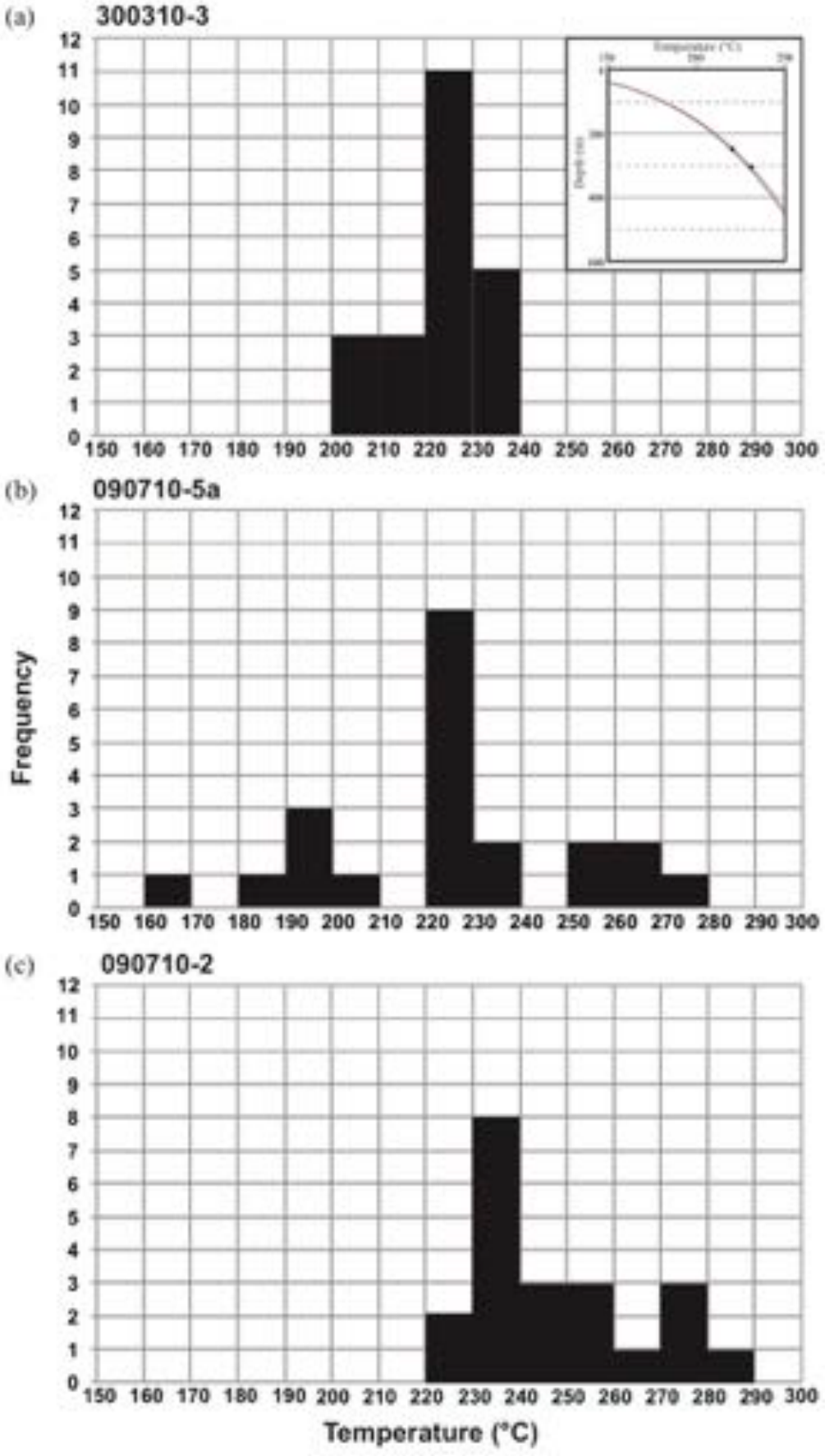
(a)
300310-3
(b)
090710-5a
(c)
090710-2
Frequency
Temperature (°C)
0 1 2 3 4 5 6 7 8 9 10 11 12
150 160 170 180 190 200 210 220 230 240 250 260 270 280 290 300

Fig. 10

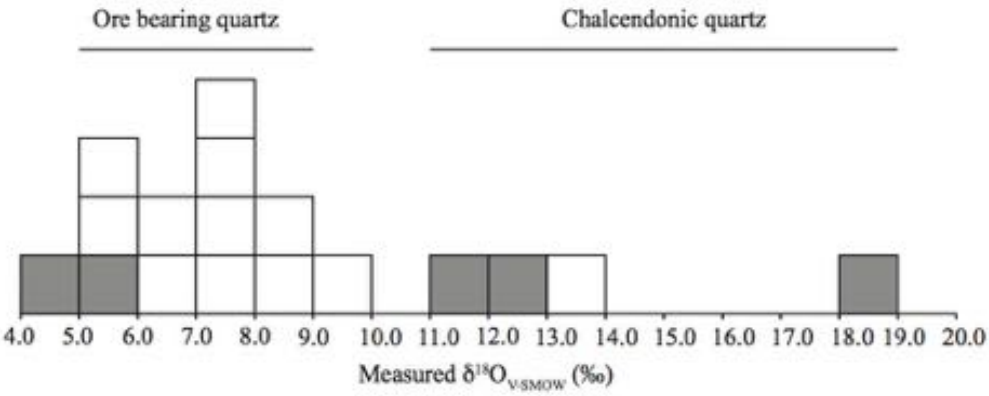
Ore bearing quartz
Chalcendonic quartz
4.0 5.0 6.0 7.0 8.0 9.0 10.0 11.0 12.0 13.0 14.0 15.0 16.0 17.0 18.0 19.0 20.0
Measured δ18OV-SMOW (‰)

Fig. 11

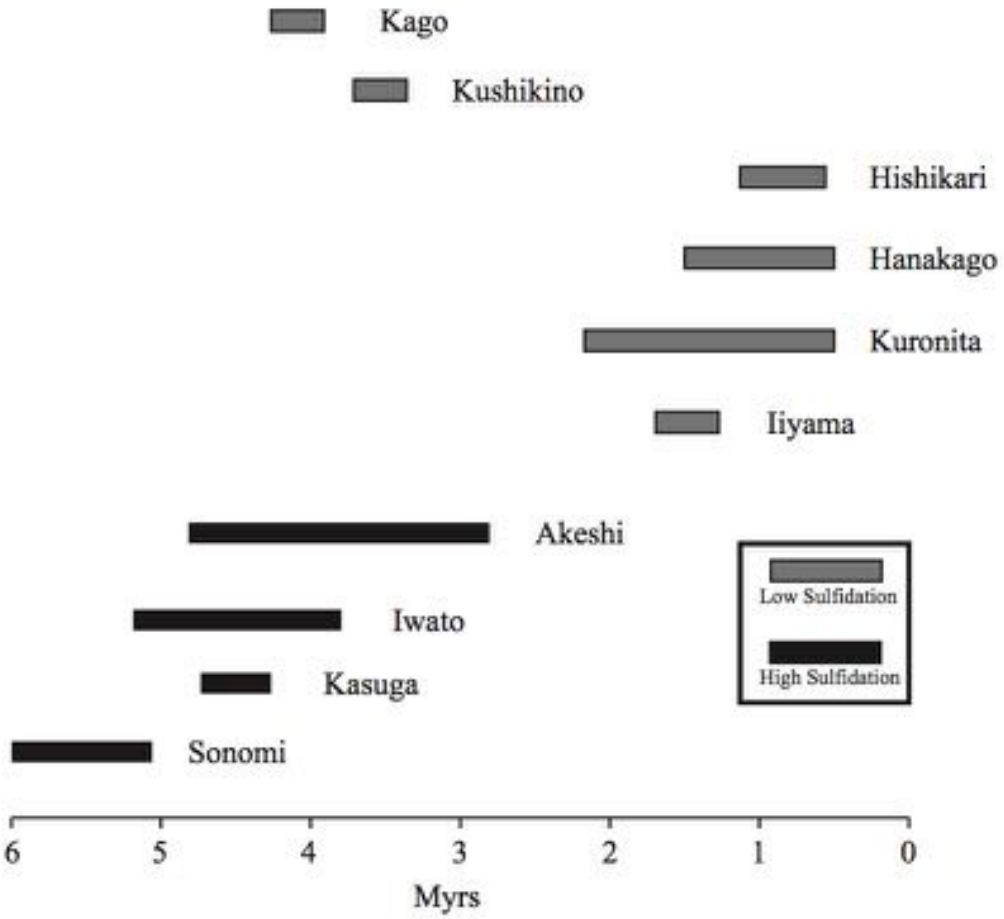
Kago
Kushikino
Hishikari
Hanakago
Kuronita
Iiyama
Akeshi
Iwato
Kasuga
Sonomi
Low Sulfidation
High Sulfidation
6
5
4
3
2
1
0
Myrs

Fig. 12

Age data for major deposits in the Nansatsu district

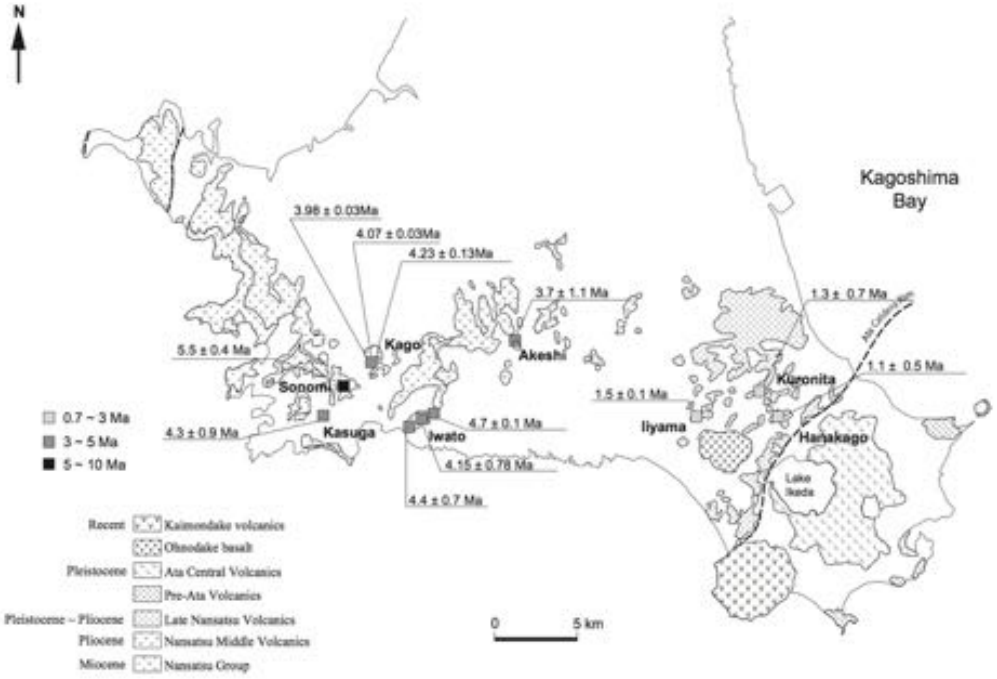

Fig. 13

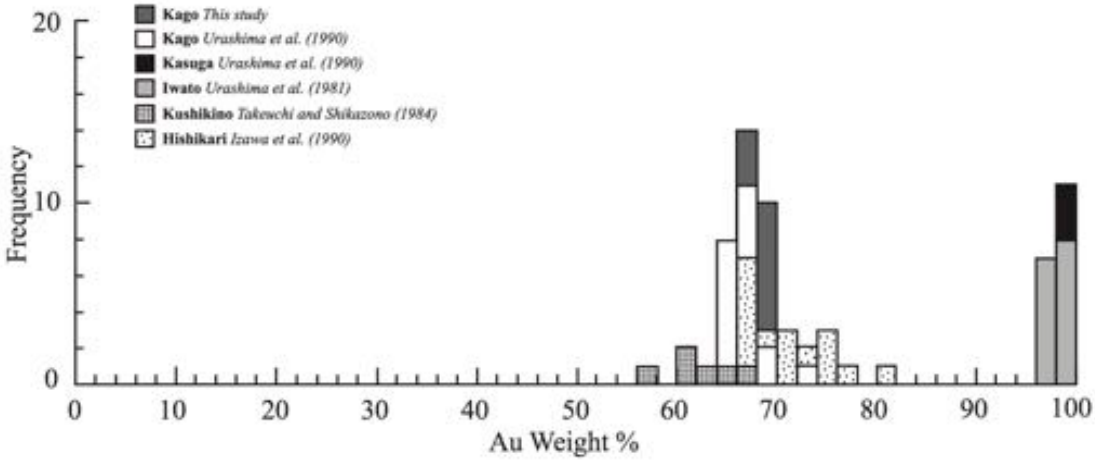
Kago This study
Kago Urashima et al. (1990)
Kasuga Urashima et al. (1990)
Iwato Urashima et al. (1981)
Kushikino Takeuchi and Shikazono (1984)
Hishikari Izawa et al. (1990)
Frequency
20
10
0
0
10
20
30
40
50
60
70
80
90
100
Au Weight %

Fig. 14